Åbo Akademi University

Application of Hydrophobic Solid Contacts in Ion-Selective Electrodes

Ning He

Laboratory of Analytical Chemistry
Johan Gadolin Process Chemistry Centre
Faculty of Science and Engineering
Åbo Akademi University
Åbo, Finland, 2017

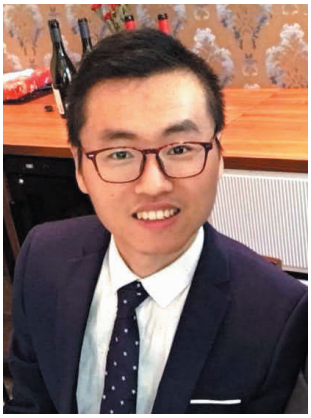

Ning He

Born 1987 in Xi’an, China
M.Sc. at the Laboratory of Industrial Chemistry and Reaction Engineering, Åbo Akademi University (ÅAU), 2008.
Worked at the Laboratory of Physical Chemistry at ÅAU during 2009-2010.
Joined the Laboratory of Analytical Chemistry at ÅAU in Oct. 2010

Faculty of
Science and Engineering

Johan Gadolin
Process Chemistry Centre

Application of Hydrophobic Solid Contacts in Ion-Selective Electrodes

Ning He

Laboratory of Analytical Chemistry
Johan Gadolin Process Chemistry Centre
Faculty of Science and Engineering
Åbo Akademi University
Åbo, Finland, 2017

Supervised by

Docent *Tom Lindfors (supervisor)*
Åbo Akademi University
Faculty of Science and Engineering
Johan Gadolin Process Chemistry Centre
Laboratory of Analytical Chemistry
Åbo, Finland

and

Docent *Rose-Marie Latonen (co-supervisor)*
Åbo Akademi University
Faculty of Science and Engineering
Johan Gadolin Process Chemistry Centre
Laboratory of Analytical Chemistry
Åbo, Finland

Reviewer

Professor Konstantin N. Mikhelson
St. Petersburg State University
Chemistry Institute
Ion-Selective Electrode Laboratory
St. Petersburg, Russia

and

Professor Leif Nyholm
Uppsala University
Department of Chemistry - Ångström Laboratory
Inorganic Chemistry
Uppsala, Sweden

Opponent

Professor Konstantin N. Mikhelson
St. Petersburg State University
Chemistry Institute
Ion-Selective Electrode Laboratory
St. Petersburg, Russia

ISBN: 978-952-12-3593-1 (Print)
ISBN: 978-952-12-3594-8 (PDF)
Painosalama Oy - Åbo, Finland 2017

- 过去心不可得，现在心不可得，未来心不可得

Neither the past, the present nor the future mind can be found.

- 以无我、无人、无众生、无寿者，修一切善法,

则得阿耨多罗三藐三菩提.

The practice of all good virtues (Dharma), free from attachment to an ego, a personality, a being and a life, will result in the attainment of Supreme Enlightenment.

----《金刚般若波罗密多经》

《THE DIAMOND SUTRA》

Table of contents

Preface

The research work was mainly carried out at the Laboratory of Analytical Chemistry, Åbo Akademi University, Turku, Finland. Paper III and Paper IV were done in collaboration with Prof. Róbert E. Gyurcsányi at the Department of Inorganic and Analytical Chemistry, "Lendület" Chemical Nanosensors Research Group, Budapest University of Technology and Economics, Budapest, Hungary. The Academy of Finland (project numbers 260036, 130588 and 263656), Åbo Akademi University, Oskar Öflunds Stiftelse, Johan Gadolin Process Chemistry Centre and Graduate School of Chemical Sensors and Microanalytical System (CHEMSEM) are gratefully acknowledged for financial support.

I wrote the preface at last, and felt so excited about saying grateful words to so many people who helped me in the past few years.

Firstly, I want to start by thanking my supervisors: Docents Tom Lindfors and Rose-Marie Latonen for your kind patience, support and encouragement during these years. Special thanks to Tom, without you, there would have been no PhD thesis.

I also would like to thank the head of the laboratory, Professor Johan Bobacka, for encouraging me to finalize my PhD study. Another great thanks goes to Prof. Róbert E. Gyurcsányi for the kind hospitality when I was working at your laboratory in Budapest. I still remember the wonderful time when we visited the Lake Balaton with your group. Thanks for your wisdom and guidance that helped me to carry on the research. I also wish to thank Assistant Prof. Lajos Höfler for our collaboration and for your skilful modelling work.

It is a true pleasure to work at the Laboratory of Analytical Chemistry. Special thanks to my lovely roommates, Marceline and Kai. Big G and Michal, a deep hug for sharing our stories, tears and joy. Ulriika, you are the good spirit of Analyten. I am grateful to have Tingting's laughter as the colleague and for Sten's kind assistance. Thanks Yasu for the Japan vs. China table tennis battles, Zekra, Kim and Zhanna for your patient help. Sara, I am waiting for your defence day. Narender, good luck with your PhD studies.

Without you, my friends, I would not have survived living and studying in Turku for so many years. Xiexie, to Shaoxia, Xiaoju, Pingping, Qian, Bingzhi, Tao, Nianxing, Chunlin, Duanmu, Di, Daniel, Xuehan, Yanxi, Zhiqiang, Hao, Hongyan, Nana, Haolin, Ling, Chen, Jingxin, Taotao, Dede, Ying, Xue and Wenyang. Thank you for being in my life! 感恩上苍恩赐，带你们到我身边，还有一群可爱的宝宝们！

I would like to express my deepest gratitude to my family. Mum and dad, one of my classmates in high school told me you are the best parents he met, I totally agree. Thanks for the solid love and support. Moreover, to my elder sister, let us have a deep hug when we will meet in the near future. 最深切得感恩，献给我的家人。 爸爸妈妈，曾经有个同学告诉我，说你们是他见过的最棒的父母，我发自心底的赞同。 姐姐，再见面时，让我们深情拥抱吧！

In Åbo (Turku), Finland
爱你们的宁

List of publications

Paper I. Determination of water uptake of polymeric ion-selective membranes with the coulometric Karl Fischer and FTIR-ATR techniques
N. He, and T. Lindfors, ***Anal. Chem.*** 2013, *85*, 1006-1012.

Paper II. Influence of hydrophobization of the polyazulene ion-to-electron transducer on the potential stability of calcium-selective solid-contact electrodes
N. He, L. Höfler, R.-M. Latonen and T. Lindfors, T. ***Sens. Actuators, B***, 2015, *207*, 918-925.

Paper III. Electropolymerized hydrophobic polyazulene as solid-contact in potassium-selective electrodes
N. He, R.E. Gyurcsányi, and T. Lindfors, ***Analyst***, 2016, *141*, 2990-2997.

Paper IV. Pre-polarized hydrophobic conducting polymer solid-contact ion-selective electrodes with improved potential reproducibility
N. He, S. Papp, T. Lindfors, L. Höfler, R.-M. Latonen and R.E. Gyurcsányi, ***Anal. Chem.***, 2017, *89*, 2598-2605.

Contributions of the author

Paper I: The author participated in planning of experiments, did all the experimental work and wrote the first draft of the manuscript.

Paper II: The author participated in planning of experiments, did all the experimental work except for the mathematical modeling and wrote the first draft of the manuscript.

Paper III: The author participated in planning of experiments, did all the experimental work and wrote the first draft of the manuscript.

Paper IV: The author participated in planning of experiments, did the experimental work except for the determination of the upper detection limit and selectivity coefficients, the mathematical modeling and interpretation of the vibrational bands in the FTIR-ATR spectra, and wrote the first draft of the manuscript.

Publications related to the topic

1. Transportation and Accumulation of Redox Active Species at the Buried Interfaces of Plasticized Membrane Electrodes
   M. Sohail, R. De Marco, Z. Jarolímová, M. Pawlak, E. Bakker, N. He, R. -M. Latonen, T. Lindfors, J. Bobacka, ***Langmuir***, 2015, *31*, 10599-10609.

2. Paper-based microfluidic sampling and separation of analytes for potentiometric ion sensing
   J. Ding, N. He, G. Lisak, W. Qin, J. Bobacka, ***Sens. Actuators, B***, 2017, *243*, 346-352.

3. Electrosynthesized polypyrrole/zeolite composites as solid contact in potassium ion-selective electrode
   K. Yu, N. He, N. Kumar, N. Wang, J. Bobacka, A. Ivaska, ***Electrochim. Acta***, 2017, *228*, 66-75.

4. Influence of phosphate buffer and proteins on the potentiometric response of a polymeric membrane-based solid-contact Pb(II) ion-selective electrode
   N.K. Joon, N. He, M. Wagner, M. Cárdenas, J. Bobacka, G. Lisak, ***Electrochim. Acta***, *in press*, DOI: 10.1016/j.electacta.2017.08.126.

Abbreviations

ACN	acetonitrile
CA	contact angle
CV	cyclic voltammetry
CWE	coated-wire electrode
DIW	deionized water
DOS	bis(2-ethylhexyl)sebacate
ECP	electrically conducting polymer
EMF	electromotive force
ETH 1001	diethyl n,n′-[(4*r*,5*r*)-4,5-dimethyl-1,8-dioxo-3,6-dioxaoctamethylene] bis(12-methylaminododecanoate) (calcium ionophore I)
ETH 5234	10,19-bis[(octadecylcarbamoyl)methoxyacetyl]-1,4,7,13,16-pentaoxa-10,19-diazacycloheneicosane (calcium ionophore IV)
FIM	fixed interference method
FTIR-ATR	Fourier Transform Infrared Attenuated Total Reflection
LDL	lower detection limit
MPM	matched potential method
IR	infrared
IRAV	infrared active vibration
IRE	internal reflection element
ISE	ion-selective electrode
ISM	ion-selective membrane
o-NPOE	2-nitrophenyl octyl ether
PANI	polyaniline
PAz	polyazulene
PEDOT	poly(3,4-ethylenedioxythiophene)
PEEK	polyether ether ketone
$PFOS^-$	perfluorooctanesulfonate
POT	poly(3-octylthiophene)
PPy	polypyrrole
PVC	poly(vinyl chloride)
RE	reference electrode
SC	solid-contact
SC-ISE	solid-contact ion-selective electrode
SD	standard deviation
SR	silicone rubber
SSM	separate solutions method
THF	tetrahydrofuran
KF	Karl Fischer

KTFPB	potassium tetrakis[3,5-bis(trifluoromethyl)phenyl]borate
UDL	upper detection limit
WE	working electrode

Abstract

Ionophore-based ion-selective electrodes (ISEs) are attractive tools for environmental monitoring, process control and clinical analysis. Recent developments in ISE research, such as single-use disposable sensors, require a cost-effective miniaturized electrode design. Replacing the internal filling solution of conventional ISEs by a suitable ion-to-electron transducer is one of the main challenges in fabricating robust, driftless and maintenance-free potentiometric solid-contact ion-selective electrodes (SC-ISEs). Due to their cost-effectiveness and easy fabrication, electrically conducting polymers (ECPs) applied as the ion-to-electron transducer for ISEs offer a promising solution to fabricate SC-ISEs. However, the water layer formation at the interface between the ion-selective membrane (ISM) and the solid-contact (SC) and the SC | electrode substrate interface results in potential instability of the ECP-based SC-ISEs. To eliminate the water layer formation, the use of hydrophobic ISMs and SCs is recommended.

In this work, the hydrophobicity and water uptake properties of the ISMs were studied by the Fourier transform infrared spectroscopy attenuated total reflection (FTIR-ATR) technique and the oven-based coulometric Karl Fischer titrations. The water uptake of plasticized polyvinyl chloride (PVC) and silicone rubber (SR) based ISMs was compared. Furthermore, the hydrophobic polyazulene (PAz) was introduced for the first time as the SC layer in SC-ISEs, because it was found that PAz had a relatively high water contact angle (CA) in its semiconducting form (98±11º). The K^+-selective ISEs with pre-polarized PAz (at $E \leq 0.2$ V) applied as the SC showed significantly improved potential stability when they were for the first time contacted with electrolyte solution. The reproducibility of their standard potential, E^0, (SD $\leq \pm 7.9$ mV, n=4) was also improved by the pre-polarization. Moreover, the hydrophobic perfluorinated anion-doped polypyrrole (PPy-PFOS) was chosen as the SC in K^+-selective electrodes in further studies since PPy-PFOS is hydrophobic in its conducting form, contrary to most other ECPs, which are hydrophilic due to the charged polymer backbone. The pre-polarized PPy-PFOS based K^+-SC-ISEs had a very small standard deviation of E^0 (±0.7 mV, n=4), which is the best E^0 reproducibility reported for ECP-based SC-ISEs. For both the PAz and PPy based SC-ISEs, no evidence of water layer formation was found, which is beneficial for their long-term stability.

Referat

Jonoforbaserade jonselektiva elektroder kan användas för miljömonitorering, processkontroll och klinisk analys. Framsteg som nyligen gjorts inom forskningsområdet – såsom utveckling av engångssensorer – förutsätter att små elektroder kan tillverkas billigt. Vid tillverkning av jonselektiva elektroder med fast kontakt måste den inre lösningen i konventionella jonselektiva elektroder ersättas med ett fast material som har jon-till-elektronöverförings-egenskaper. Det här är den största utmaningen vid tillverkning av robusta, drift- och underhållsfria jonselektiva elektroder. Elektriskt ledande polymerer som är billiga och enkla att tillverka kan med fördel användas som jon-till-elektronöverförare i potentiometriska jonselektiva elektroder med fast kontakt. Trots många fördelar med elektriskt ledande polymerer är det möjligt att ett vattenskikt bildas mellan den jonselektiva membranen och den fasta kontakten och/eller den fasta kontakten och elektrodsubstratet. Vattenskiktet kan leda till responsinstabilitet för jonselektiva elektroder. Det är dock möjligt att förhindra vattenskiktsbildningen genom användning av hydrofoba material vid tillverkning av den jonselektiva membranen och den fasta kontakten.

I denna doktorsavhandling har jonselektiva membraners hydrofobicitet och vattenupptagning undersökts med intern reflektion FTIR-spektroskopi och den coulometriska Karl Fischer titreringstekniken. Vattenupptagningen för jonselektiva elektroder gjorda av mjukgjord poly(vinylklorid) och silikongummi har jämförts i avhandlingsarbetet. Utöver detta har den ledande polymeren polyazulen (PAz) använts för första gången som jon-till-elektronöverföringsskikt i jonselektiva elektroder med fast kontakt. Fördelen med PAz är den relativt höga vattenkontaktvinkeln (98±11°) i dess halvledande form. K^+ jonselektiva elektroder med förpolariserad PAz som fast kontakt ($E \leq 0.2$ V) uppvisade en betydligt förbättrad potentialstabilitet då elektroderna för första gången placerades i kontakt med elektrolytlösning. Reproducerbarheten för elektrodernas standardreduktionspotential (E^0) förbättrades också av förpolariseringen (SD ≤ ±7.9 mV, n=4).

Hydrofob polypyrrol (PPy) dopad med perfluoroktansulfonsyra (PPy-PFOS) användes i fortsatta studier som fast kontakt i kalium-selektiva jonselektiva elektroder. Fördelen med PPy-PFOS är dess höga hydrofobicitet i den elektriskt ledande formen i motsats till de

flesta andra elektriskt ledande polymerer som är hydrofila. E^0-reproducerbarheten för förpolariserade jonselektiva elektroder med PPy-PFOS som fast kontakt var i bästa fall ±0.7 mV (n=4). Ingen vattenlagerbildning kunde observeras för PAz- och PPy-baserade jonselektiva elektroder vilket är bra för deras långtidsstabilitet.

1. Introduction

Potentiometric ion-selective electrodes (ISEs) are an important subgroup of electrochemical sensors, which convert the activity of target ions into a measurable electronic signal[1-4]. The ion-selective membrane (ISM) as the outmost layer of the ISE provides the selectivity to the target ions. Due to their portability, simplicity, miniaturization possibility, low cost and low energy consumption, ISEs have attracted the interest of researchers all over the world. ISEs can be used for onsite and offsite monitoring in the fields of environmental analysis, quality control and clinical diagnostics. Especially, their excellent accuracy for concentration determination in clinical analysis of blood electrolytes is considered as one of the most successful applications.

Very recently, applications such as potentiometric bioassays[5-7], portable paper based platforms[8-10] and wearable sensors[11,12] have attracted much interest. For the potentiometric biosensing systems, the ISEs are usually used as indicator electrodes for protein monitoring. For example in the work of Chumbimuni-Torres et al., the concentration change of Ag^+ released from the precipitated silver on Au nanoparticles indicates the reaction of antigens with antibodies[6]. Ion-selective paper electrodes provide affordable and disposable tools for resource-limited environments[8,13,14]. The tattoo-based potentiometric ion sensors for epidermal pH monitoring[11] or wearable sensor arrays for *in situ* perspiration analysis[12] open a door to affordable continuous personal health monitoring in the near future. These applications benefit greatly from ISEs having a solid internal contact (SC-ISEs)[15].

Based on the material used for the ion-selective membrane (ISM), ISEs are classified as glass, crystalline and polymeric membrane ISEs. Glass ISEs with the ISM mainly consisting of silicate glasses are the oldest and most frequently used and are considered as the best pH sensors. The most well-known type of crystalline ISEs is the fluoride electrode based on a lanthanum fluoride monocrystalline membrane[4]. However, ISEs with polymeric ISMs are available for a large number of ions and will be discussed in this thesis.

The aim of this Ph.D. work is to determine the water uptake of the polymeric ISMs and improve the reproducibility and potential stability of ISEs. The water layer formation underneath the ISM has been proved to be one of the major parameters that influence the potential stability of ISEs impeding their commercialization[16]. Therefore, the water uptake of poly(vinyl chloride) and silicone rubber (SR) has been studied by the FTIR-ATR and coulometric Karl Fischer (KF) titration techniques. Moreover, the different hydrophobic solid-contact (SC) materials has been used to minimize the detrimental influence from the water uptake of the ISM. For the first time, hydrophobic polyazulene (PAz) has been used as SC in solid-contact ion-selective electrodes (SC-ISE). The pre-polarized PAz-based K^+-SC-ISEs showed that the E^0 variation in the worst case was ±7.9 mV (n=4). Furthermore, polypyrrole (PPy) doped with the hydrophobic perfluorinated anion was hydrophobic at its oxidized state. ISEs having this hydrophobic PPy as SC obtained superior potential stability and piece-to-piece reproducibility compared with other electrically conducting polymer (ECP) based SC-ISEs.

2. Potentiometric ion-selective electrodes

This chapter describes the different types of ISEs, the ISM components, and the working mechanism of ISEs. Moreover, it introduces the important characteristic parameters of ISEs.

2.1. General

ISEs have the longest history among the chemical sensors, starting from 1906[17] when it was observed that the potential of a glass membrane depends on the proton concentration, *i.e.* making it pH-sensitive. The polymeric membrane based ISEs, incorporating ionophores functioning as the complexing agent, nowadays constitute the major group of the ISEs. By using the ionophore-based polymeric ISM, different types of ISEs have been designed, as summarized in **Figure** 1.

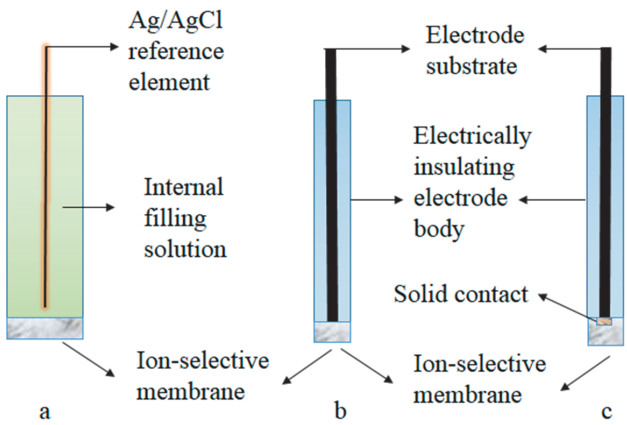

Figure 1. Different types of ISEs: a) conventional ISE with an internal Ag/AgCl reference element and internal filling solution, b) coated-wire ISE, c) ISE with a solid-contact layer

The conventional ISE, which consists of an ISM, internal reference electrode and internal filling solution, is presented in **Figure** 1a[4,17]. The internal solution can be an electrolyte solution or gel[18]. Most often, the Ag/AgCl is used as the internal reference electrode. For example, in the conventional K^+-selective ISEs, a typical internal filling solution is 0.01 M KCl[4]. As one big step towards solid-state ISEs, the so-called coated-wire ISEs (CWEs)

(**Figure** 1b) were invented in the 1970s[19]. They have a simple design with the ISM deposited directly onto the conductive electrode substrate. However, due to the blocked charge transfer and the ill-defined interfacial potential between the ionically conducting ISM and the electronically conducting electrode substrate, CWEs have an unstable potential and a low reproducibility. Moreover, a water layer will form on the electrode substrate and cause transmembrane fluxes of ions. To improve the performance of the CWEs, an intermediate layer with redox and ion-exchange properties is needed between the electrically conducting substrate and the ISM[20]. As can be seen in **Figure** 1c, the solid-contact ISEs (SC-ISEs) consist of an SC layer functioning as an ion-to-electron transducer. The SC-ISEs will be discussed in detail in *Chapter* 3**.**

2.2. Ion-selective membranes

The ISMs make the ISEs selective to a specific cation or anion[1,2,4,17]. The ISMs are typically composed of an ionophore, a lipophilic ion exchanger and polymeric matrix with or without plasticizer. Normally, the ionophore content is 0.5-2 wt % of the ISM dry mass[4]. The types of ionophore and the lipophilic ion exchangers and their ratios determine the selectivity value of the ISM[4]. The plasticizers provide elasticity to the ISMs by lowering the glass-transition temperature of the polymeric matrix[4]. Moreover, the plasticizers enhance the solubility of the ionophore in the ISM and also the mobility of the ionophore-ion complex in the ISM[4]. The cocktail solution for the fabrication of the ISM is made by dissolving all the membrane components into a volatile solvent such as tetrahydrofuran (THF). The ISMs are then prepared by casting the cocktail solution: (i) onto a glass substrate and after drying they are cut to suitable sizes for the fabrication of conventional ISEs, (ii) directly onto the electrode body and substrate for CWEs or (iii) onto the substrate coated with the SC for SC-ISEs. The cocktail solution will form the ISM after the evaporation of THF overnight for plasticized polyvinyl chloride (PVC) or after 72 h for silicone rubber (SR).

Ionophore

The ionophores are usually either electrically charged or neutral and they determine the selectivity of the ISM by their relatively strong and reversible binding to the analyte ion[1,2,4,17]. Their formal complex formation constants are in the range of 10^{8}-10^{13} kg mol^{-1}

for monovalent analyte ions and 10^{15}-10^{29} kg^2 mol^{-2} for divalent ions[21]. The selective binding process generates the potential difference at the interface of the ISM | sample solution and forms the phase-boundary potential[17]. In the ideal case, the ionophore does not form any complexes with the interfering ions. However, too strong complexation of analyte ion will result in the extraction of counter ions from the sample solution, known as Donnan exclusion failure. The best-known ionophore used for cation determination was the neutral carrier valinomycin, which is selective to K^+ ions[2,22]. This ionophore has an electron-rich cavity in the center and therefore selectively extracts K^+ ions due to the size fit of the cavity and the K^+ ion. Due to the high selectivity, the valinomycin-based ISEs are widely used in clinical analysis[17]. In *paper III* and *IV*, the valinomycin-based K^+-selective SC-ISEs were investigated while in *paper I* and *II*, the calcium ionophore I (ETH 1001) and IV (ETH 5234) were used in Ca^{2+}-selective ISMs.

Lipophilic ion exchangers

In the case of neutral ionophores, the lipophilic ion exchangers are needed to exclude co-extraction of electrolytes from sample solution. In cation-selective ISEs, the lipophilic ion exchanger can dissociate into a lipophilic organic anion and a hydrophilic cation in the membrane phase[4,23]. Due to its lipophilicity, the organic anion is confined in the membrane phase and does not diffuse to the interface of the ISM | sample solution. The lipophilic organic anion provides the ion-exchanger sites in the membrane, while the hydrophilic cation is able to cross the interface (to preserve the electroneutrality of the ISM upon complexation of the primary ion from the solution). The lipophilic anions prevent the co-extraction of oppositely charged counter ions from the aqueous electrolytes, which is called Donnan exclusion[4]. Because of the macroscopic electroneutrality in fully conditioned cation-selective ISMs (*e.g.* based on a neutral carrier), the positive charge of the ion-ionophore complexes must be equal to the negative charge of the ion-exchanger sites. Typically, the molar ratio between the ionophore and the lipophilic ion exchanger is higher than one, resulting in the absence of free hydrophilic cations in the ISM, since in practise all analyte cations in the membrane phase form complexes with the ionophore if the complexation stoichiometry is 1:1[24]. The optimized molar ratio between the ionophore and the lipophilic ion exchanger for

obtaining the best selectivity depends on the stoichiometry ratio of the primary ion-ionophore complexes[24].

The selectivity of ISMs containing only the ion-exchanger (but not the ionophore) follows the Hofmeister series which is a measure of the lipophilicity of anions and cations (solubility of ions in proteins and macromolecules)[25]:

$$\text{Large lipophilic anions} > ClO_4^- > SCN^- > I^- > NO_3^- > Br^- > Cl^- > HCO_3^- > SO_4^-$$

$$\text{Large lipophilic cations} > Cs^+ > K^+ > NH_4^+ > Na^+ > Li^+ > Sr^{2+} > Ca^{2+} > Mg^{2+}$$

The lipophilic ion-exchanger used in this work was potassium tetrakis[3,5-bis(trifluoromethyl)phenyl]borate (KTFPB). For example in Ca^{2+}-selective ISMs incorporating KTFPB as the ion-exchanger, the Ca^{2+} ions partition from the aqueous phase to the membrane phase and complex with the ionophore during the conditioning in high concentration Ca^{2+} solution. As the result of the complexation, the K^+ ions from KTFPB are expelled from the ISM to the aqueous phase to preserve the macroscopic electroneutrality of the ISM.

Polymeric matrices and plasticizers

Normally, the content of the ionophore and lipophilic salt is only a few percent of the whole membrane dry weight, while the major part consists of the plasticized or non-plasticized polymer matrix[4]. In *paper I*, we used Ca^{2+}-selective plasticized PVC-based ISMs consisting of 32.92% (w/w) PVC, 65.83% bis(2-ethylhexyl)sebacate (DOS), 0.45% KTFPB and 0.8% calcium ionophore IV (CaISM(IV-PVC)) or calcium ionophore I (CaISM(I-PVC)), but also SR-based Ca^{2+}-selective ISMs consisting of 98.1% (w/w) RTV 3140, 0.9% KTFPB and 1.0% calcium ionophore I (CaISM(I-SR)). In *paper II - IV*, we prepared K^+-selective plasticized PVC-based ISMs consisting of 32.9% (w/w) PVC, 65.7% bis(2-ethylhexyl)sebacate, 1.0% valinomycin and 0.4% KTFPB. The thickness of the ISMs depends on the dry mass of the membrane cocktail solution, the volume of the cocktail solution applied on the electrode surface and also on the surface area of the substrate. Typically, it was ca. 100-300 μm.

Plasticized PVC is the most popular membrane matrix for ISMs. Typically, the mass ratio of the plasticizer to PVC is 2:1[4]. The most commonly used plasticizers are esters, such as DOS, 2-nitrophenyloctyl ether and other ethers[1,2]. Plasticizers decrease the ohmic resistance and increase the elasticity of the ISM, and also improve the solubility of the ionphores in the ISM. However, the plasticized PVC-based ISMs suffer from the leaching of the plasticizer[26,27], ionophore[28] and lipophilic salt from the ISM to the solution phase[29]. Also in PVC and SR-based ISMs, the water content in the conditioned ISMs can be ca. 0.5-2% (w/w), which can increase the inhomogeneity of ISMs[4,30,31]. Because of the water uptake, the lifetime of the ISEs and their potential stability will be limited. Therefore, finding new hydrophobic membrane matrix materials for the ISM fabrication to replace plasticized PVC, as well as covalently binding the ionophores and/or the lipophilic ionic sites to the PVC backbone has attracted considerable attention[4]. The hydrophobic ISM restrains the leaching of the membrane components and decreases its water uptake.

A specific type of SR which can vulcanize at room temperature, is one of the suitable substitutes for PVC[32,33], since it has a good adhesion to the electrode substrate and excellent mechanical properties. The SR-based electrodes also show enhanced lifetime and good piece-to-piece reproducibility[33-35]. In *paper I*, the Dow Corning RTV 3140 was used to fabricate the SR-based Ca^{2+}-selective ISMs without plasticizers and the water uptake of this type of ISMs was determined. However, the SR-based ISM suffers from the high resistance, which results in high sensitivity to electrical disturbances, but also from the poor solubility of some ionophores and lipophilic ion exchangers. These disadvantages of SR-based ISEs make them suitable for only a limited number of analytes[36]. Hence, a hybrid PVC-SR-based ISM was used for hydrogen-selective ISEs[37]. It was shown that the lifetime of the ISEs was extended by adding 10.0 wt% SR into the PVC matrix.

2.3. Working mechanism of potentiometric ion-selective electrodes

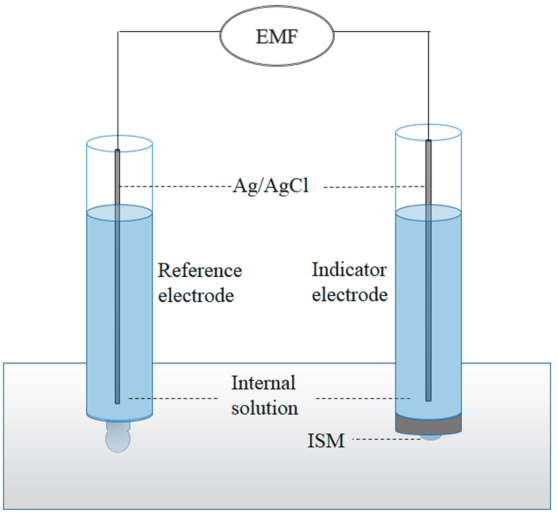

Figure 2. A schematic figure illustrating the electrochemical cell that is used in potentiometric measurements.

The electrochemical cell consists of two electrodes: the reference electrode (RE) and the indicator electrode. As shown in **Figure** 2, a conventional ISE typically consists of an Ag | AgCl wire as the inner reference element in contact with the inner filling solution and an ISM as the outermost membrane.

In potentiometry, the potential difference, *i.e.* the electromotive force (EMF), is measured by passing a current in the picoampere range between the indicator electrode and RE when they are immersed into a solution[1,2,4,15,17]. The potential of the indicator electrode must depend only on the activity of the analyte ion, while the RE provides a defined constant potential. The electrochemical cell describing the conventional potentiometric ISE can be written as:

Cu | Ag | AgCl | 3 M KCl || sample | ISM | Internal solution | AgCl | Ag | Cu

where the RE is written to the left and the ISE to the right, and they are connected by Cu contacts to an mV-meter with a high input impedance.

Phase boundary potential model

The phase boundary potential (E_{PB}) model requires two assumptions. One is that the diffusion potential in the ISM is neglected*, i.e.* the E_{PB} governs the potential of the ISE[13,24,38]. In other words, there are no concentration gradients in the membrane. The other is called *the total equilibrium assumption*, which assumes that an electrochemical equilibrium is achieved at the sample | ISM interface and also in the ISM[13,15,24]. Based on these two assumptions, the EMF, which is the sum of all interfacial potentials in the electrochemical cell, can be described by Eq. 1[13,15,24] .

$$\mathrm{EMF} = E_J + E_{PB(ISM/sample)} + E_{const} \qquad \text{(Eq. 1)}$$

where E_J is the liquid-junction potential of the RE, $E_{PB(ISM/sample)}$ is the phase boundary potential at the ISM | sample solution interface and E_{const} is the sum of the other sample-independent potentials, such as the phase boundary potential at ISM | internal solution interface[13,15,24] .

At thermodynamic equilibrium, the electrochemical potentials in the sample solution and the ISM must be equal. The electrochemical potential $\tilde{\mu}_i$ of species *i* in phase α is defined as[15,17,22]:

$$\tilde{\mu}_i = \mu_i + z_i F \phi_i = \mu_i^0 + RT \ln(a_i) + z_i F \phi_i \qquad \text{(Eq. 2)}$$

where μ_i^0 is the standard chemical potential, a_i is the activity, z_i is the valency, ϕ_i is the electrical potential, R is the universal gas constant, T is the absolute temperature and F is the Faraday constant.

Hence, $E_{PB(ISM/sample)}$ can be derived for species *i* as[15,17,22,24]:

$$E_{PB(ISM/sample)} = \Delta\phi = \phi^M - \phi^S = \frac{\mu_i^{0,S} - \mu_i^{0,M}}{z_i F} + \frac{RT}{z_i F} \ln \frac{a_i^S}{a_i^M} \qquad \text{(Eq. 3)}$$

where superscripts M and S stand for the ISM and solution phase, respectively. ϕ^M and ϕ^S are the electrical potentials, $\mu_i^{0,M}$ and $\mu_i^{0,S}$ are the standard chemical potentials, and a_i^M and

a_i^S are the activities in these two phases. Since the ionophore complexes selectively most of the analyte ions, the activity of the free analyte ions (a_i^M) in the ISM can be assumed to be constant. Thus, the sum of all sample-independent parameters can be described as a constant E^0, which includes the chemical standard potential from each phase[3,9,21,23]. By inserting Eq. 3 into Eq. 1, under the assumptions made above, at 25 °C, it gives[9,21,23]:

$$\mathrm{EMF} = E_J + E^0 + \frac{59.16\ \mathrm{mV}}{z_i} \log a_i^S \qquad \text{(Eq. 4)}$$

This well-known equation is called the Nernst equation. The response of the ISE depends only on the changes in a_i^S, which is the activity of the analyte ion *i* in sample solution, rather than its concentration. The activity corresponding to a given concentration can be calculated by the extended Debye-Hückel equation[39].

E_J, which is called the liquid-junction potential, occurs due to the charge separation at the liquid junction formed between the inner solution of the reference electrode (commonly 3 M KCl) and the sample/standard solution. E_J is caused by the differences in ion mobilities of cations and anions in solution. It is formed, for example, in the porous glass frit of the RE. Generally, there are two types of REs, i.e. *single-junction* and *double-junction* REs. Commonly, the *single-junction* RE has an Ag/AgCl wire immersed in 3 M KCl solution (internal solution). The high concentration of KCl solution causes that the ion transportation at the porous glass frit to be dominated by the K^+ and Cl^- ions with almost similar mobilities and the liquid junction potential is thus minimized. Furthermore, the constant concentration of Cl^- in the inner reference solution provides a stable potential for the RE. A way of finely circumventing the contamination of the sample solution by the KCl solution of the RE is to add a salt bridge solution between the internal filling solution and the sample solution. The bridge solution for the *double-junction* RE is usually lithium acetate (CH_3COOLi) which has similar cation and anion mobilities and minimizes the liquid junction potential[4,22]. The value of the liquid junction potential can be estimated by the Henderson equation[22,40]:

$$E_J = \frac{\sum \frac{|z_i|\, u_i}{z_i} (C_{i,\mathrm{ref}} - C_{i,S})}{\sum |z_i|\, u_i\, (C_{i,\mathrm{ref}} - C_{i,S})} \frac{RT}{F} \ln \frac{\sum |z_i|\, u_i\, C_{i,S}}{\sum |z_i|\, u_i\, C_{i,\mathrm{ref}}} \qquad \text{(Eq. 5)}$$

where u_i is the mobility ($cm^2\ s^{-1}V^{-1}$) and z_i is the charge of species *i*, $C_{i,S}$ and $C_{i,ref}$ are the concentration of species *i* in the sample solution and internal filling solution of the single junction RE or the bridge solution of the double junction RE, respectively.

Working range and slope

For practical applications, the working range and slope of the potentiometric ISE response are important parameters, which are determined from the calibration curve. The working range is defined by the difference between the upper detection limit (UDL) and lower detection limit (LDL), as shown in **Figure** 3[4]. Typically, these detection limits are given as the intersection of two extrapolated linear lines at the high activity range for UDL and low activity range for LDL. The UDL is determined by the coextraction of primary ions together with counter ions from the aqueous sample solution into the ISM[4]. As a result, $a_{i,}^{M}$ in Eq. 3 increases and the measured EMF is lower than that calculated from the ideal Nernst equation[4]. On the other hand, the value of the LDL is mainly influenced by the zero-current transmembrane ion fluxes, *i.e.* the leaching of the primary ions from the ISM phase to the sample solution or the transportation of the interfering ions from the sample solution to the ISM phase. There are several methods to reduce these detrimental ion fluxes. One method is to decrease the ion fluxes in the ISM phase, *i.e.* the mobilities of the ions (for example, by using membrane matrices with lower ion permeability). The other method is to increase the ion convection in the sample phase to avoid the composition change of the diffusion layer near the ISM caused by leaching of ions from the ISM (for example, by stirring the sample solution)[41]. For trace analysis and biosensing, the LDL is usually more important than the UDL.

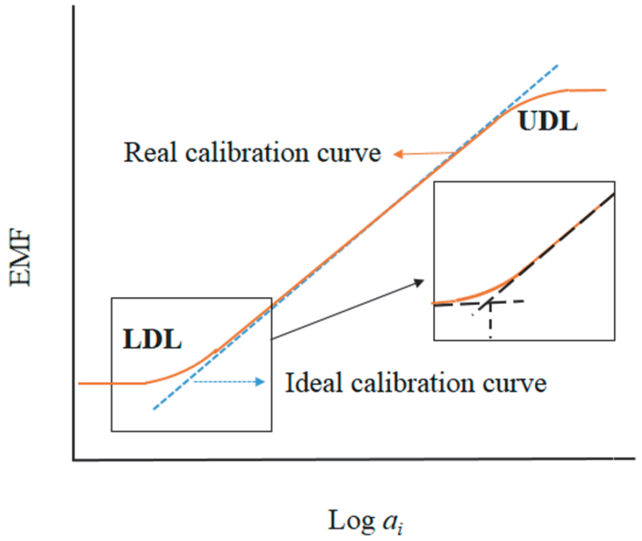

Figure 3. The graph showing the ideal calibration curve and the real calibration curve, and one way to determine the LDL.

Selectivity

Selectivity describes the influence of the interfering ions on the EMF of the ISE. The $E_{i,j}$, which is the potential difference between the RE and ISE in the solution of primary ion *i* containing also the interfering ion *j*, can be calculated by the Nikolskii-Eisenman equation:

$$E_{i,j} = E^0 + \frac{RT}{z_i F} \ln \left(a_{i,S} + K_{i,j}(a_{j,S})^{z_i/z_j}\right) \quad \text{(Eq. 6)}$$

where $a_{i,S}$ is the activity of the primary ion *i* in sample solution, z_i is the charge of ion *i*, $a_{j,S}$ is the activity of the interfering ion *j* in sample solution, z_j is the charge of ion *j*, and $K_{i,j}$ is the selectivity coefficient of *i* over *j*. Although the estimation of the selectivity coefficient relies on the Nikolskii-Eisenman equation, its determination is performed by various methods, such as the *separate solutions method* (SSM), *fixed interference method* (FIM) and *matched potential method* (MPM)[4,42]. The solutions used in the SSM are pure primary and interfering ion solutions. For the FIM, the EMF is measured in solutions of

the primary ion at different concentrations but with a constant concentration of the interfering ion. For MPM, the selectivity coefficients are determined by adjusting the electrode potentials to the same potential values in the primary or interfering ion solutions[4].

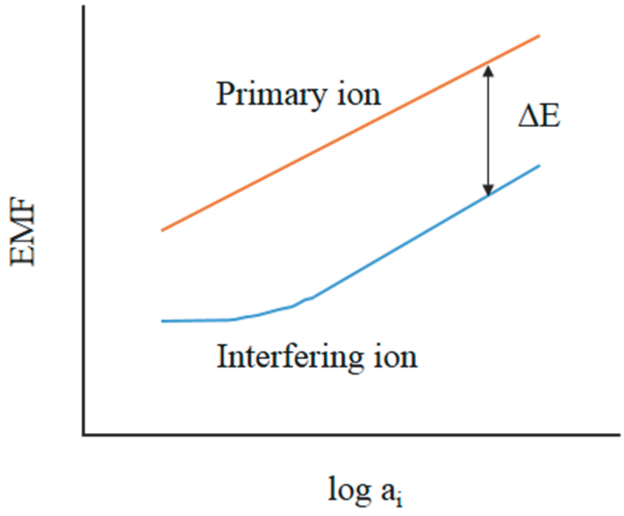

Figure 4. Figure illustrating the separate solution method (SSM).

The SSM is done by calibrating the ISE separately in pure electrolyte solutions (interfering ions first and primary ion at last) at high enough concentrations (typically 10^{-1}-10^{-4} M). As shown in **Figure** 4, the slope of the calibration curves can be determined for both the interfering ions and the primary ion. The potentiometric selectivity coefficients are obtained according to Equation 7 [1,4,42].

$$\log K_{i,j} = \frac{1}{S}\left(\mathrm{EMF_j}\text{-}\mathrm{EMF_i}\right) \log \frac{a_i}{a_j^{z_i/z_j}} \qquad \text{(Eq. 7)}$$

where S is normally the slope for the linear part of the calibration curve for the primary ion, EMF_i, and EMF_j are the EMF values of the ISE in the primary ion and the interfering ion solutions at the same concentration, respectively. The ΔE in **Figure** 4 is the EMF_i-EMF_j in Eq. 7.

To achieve a better constancy of the selectivity, the unbiased selectivity method was recommended[1,4]. Before placing the ISEs in contact with the primary ion solution, the EMF of newly prepared ISEs was first measured in the interfering ion solutions. In this way, one can be sure that the potential measured in solutions of highly discriminated interfering ions is not influenced by possible leaching of primary ion from the ISM. Hence, in this thesis, the selectivity coefficients were determined by the unbiased selectivity method[4].

3. Solid-contact ion-selective electrodes

This chapter focuses on electrically conducting polymers (ECPs) based all-solid-state ISEs. It describes the basic properties of ECPs and two specific ECPs (polyazulene, (PAz) and polypyrrole, (PPy)) used in the studies within this thesis. Furthermore, the mechanism of ECPs based SC-ISEs has been described in the last section.

3.1. General

As shown in **Figure** 2a, the conventional ISEs are with internal filling solution. Therefore, they are sensitive to the evaporation of the internal filling solution, sample temperature and pressure[4]. The next generation of ISEs is required to be robust and portable because of their use in environmental applications and point-of-care diagnostics. Replacing the liquid internal contact with a suitable SC is the major challenge for the fabrication of ISEs with the properties of low cost and easy maintenance, possible miniaturization and easy operation[4,18,20]. For widespread implementation, SC-ISEs need to have a better potential stability than their liquid contact counterparts. In the construction of the SC-ISE, an SC layer is placed between the ionically conducting ISM and the electronically conducting electrode substrate to establish a thermodynamically well-defined interface[28,15].

There are many types of electroactive materials that can serve as the ion-to-electron transducer having either high double layer capacitance or high redox capacitance[43]. Porous carbon-based materials and nanostructured metals belong to the group with high double layer capacitance. Crespo et al.[44] produced a layer of carbon nanotubes with an areal double layer capacitance of 2.5 mF cm^{-2}. ECPs and redox active species belong to the other group with high redox capacitance. The areal redox capacitance of poly(3,4-ethylenedioxythiophene) doped with PSS^- (PEDOT-PSS) is 15 mF cm^{-2} [45].

The double layer capacitance of the SC layer can be increased by using porous electroactive materials, such as three-dimensionally ordered macroporous carbon[46], carbon nanotubes[44,47], reduced graphene oxide[48-50], nanoporous gold films[51], and colloid-imprinted mesoporous carbon[10]. An asymmetric electrical capacitance is formed at the interface of the ISM and the SC. The double layer capacitance originates from the charge separation of either cations in the ISM and electrons in the SC or anions in the ISM and

holes in the carbon-based SC[47]. For these materials, the high value of capacitance reduces the potential drift of the SC-ISEs. There are some additional advantages of the carbon-based materials, such as their hydrophobicity and insensitivity to light that benefits the long-term potential stability of the SC-ISEs. However, the limitation of the carbon-based materials relies either on the difficulty of manufacturing of the SCs (three-dimensionally ordered macroporous carbon, nanoporous gold films, and colloid-imprinted mesoporous carbon) or on the high cost of the raw materials (carbon nanotubes)[52].

Redox species and ECPs possessing mixed electronic and ionic conductivity belong to the other type of SC materials with high redox capacitance[53]. The redox species, such as poly(vinyl ferrocene)[54], lipophilic silver-ligand complexes[55], Co(II)/Co(III) redox buffer[50], fullerene redox buffer layer[56], self-assembled monolayers[57,58] and doped nanoclustered thin films[59,60], have also been used as ion-to-electron transducers in SC-ISEs. Their complexity of fabrication and the need for the maintenance of their electrodes are the main disadvantages[52]. The application of ECPs as SCs in ionophore-based SC-ISEs is discussed below. Furthermore, to improve the potential reproducibility and stability of the SC-ISEs, the combinations of the materials mentioned above have been previously applied as SCs, such as the colloid imprinted mesoporous carbon combined with a lipophilic Co(II)/Co(III) redox buffer layer[61], and polyaniline doped with few-layer graphene[34].

3.2. Electrically conducting polymers

3.2.1. *Synthesis*

Generally, the ECPs can be synthesised either by chemical or electrochemical methods depending on the types and the applications of the ECPs. The chemical method is better for the large-scale production at low cost. The chemical polymerization proceeds by adding an oxidizing agent, such as $FeCl_3$ or ammonium persulfate ($(NH_4)_2S_2O_8$), to the monomer solution. Typically, the resulting polymer is obtained in the form of a thick film or as a powder[62].

However, the electrochemical method is simple and controllable. An ECP film can be produced with a controlled thickness and deposited on a conductive surface. The synthesis of the ECP films is usually performed by applying a suitable potential to oxidize the monomer and form radical cation intermediates in a two- or three-electrode electrochemical cell. The electrochemical polymerization mechanism of the p-type ECPs initiated by oxidation of 5-membered heterocycle monomers is illustrated in **Figure** 5[62]. The polymerization solution typically consists of the monomer and the electrolyte salt dissolved in a suitable aqueous or organic solvent.

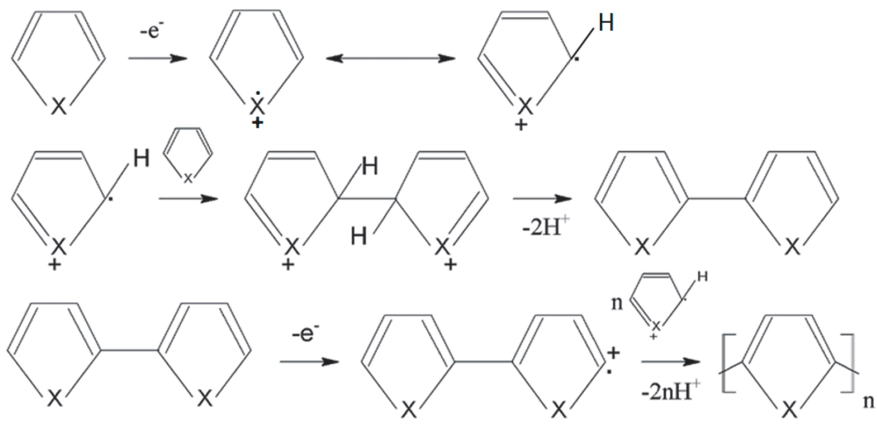

Figure 5. Electropolymerization mechanism of 5-membered heterocycles containing NH, S or O (X).

The electrochemical synthesis is performed either potentiostatically, galvanostatically or potentiodynamically[40,63]. The potentiostatic and galvanostatic methods[64] are performed at a constant potential and current, respectively. The applied potential for the potentiostatic polymerisation depends on the monomer used and is chosen at the potential regime where the oxidation of the monomer takes place. The formed film is continuously growing on the electrode surface during the polymerization and is formed in its oxidized state, because the applied potential is at the oxidation potential of the monomer and higher than that of the polymer. Both the potentiostatic and galvanostatic methods are convenient for controlling the film thickness by adjusting the polymerization time (*i.e.* controlling the amount of polymerization charge). During the potentiostatic and galvanostatic polymerization processes, side reactions, degradation or cross-linking can easily occur[65] which are difficult to control. In *paper IV*, a galvanostatic method with a constant current density of 0.25 mA cm^{-2} was used to synthesize PPy. In the potentiodynamic method, cyclic voltammetry (CV) is used to investigate the formation of the ECP during electropolymerization[40]. It is performed by scanning the potential linearly as a function of time with a constant scan rate between an anodic and a cathodic end potential[65]. In the first cycle, only the oxidation of the monomer occurs at the high potential end of the cycle. During continuous cycling, the formed radical cations start to dimerize and soluble dimers and oligomers are formed in the diffusion layer at the electrode surface according to the mechanism shown in **Figure** 5[63]. They are deposited on the electrode substrate and start to form a film by the nucleation process. The formed film shows an oxidation peak at a lower potential than the monomer and at the reverse scan, it is reduced and shows a reduction peak. During the successive potential cycling, the growing polymer continuously changes from the neutral to the conducting states, followed by the exchange of the electrolyte salt and the solvent to and from the ECP film. The film thickens by the precipitation of oligomeric intermediates formed in the solution and by the addition of the monomers and oligomers to the chain ends of the polymer[65]. The polymer matrix usually has an open structure due to the charging/discharging process[63]. In *paper II and III*, CV was used to synthesize PAz. The obtained ECPs synthesized by CV are usually at their neutral form, because the potential cycling is stopped at the potential where the polymers are in its neutral form, while the potentiostatic and galvanostatic methods produce ECPs at their oxidized form.

The properties of the ECPs, such as the surface morphology and conductivity, are affected by the polymerization method and time, temperature, solvent and electrolyte salt[62,65]. Since the electrolyte incorporates into the film as a counterion during the doping process, it is relatively easy to modify the properties of the ECPs. For instance, it was found that the polyaniline doped with the ClO_4^- ions formed a compact structure, while Cl^- ion promoted a more open structure[66]. Akieh et al. showed that the morphology of the PPy films was influenced by three different doping ions[67]. The film doped with the PSS^- ions had a dense and compact structure, while the PPy-ClO_4 film showed the cauliflower-like nodules. The PPy film doped with toluene-4-sulfonic acid monohydrate obtained a compact layer with numerous spikes. It was also demonstrated that the PPy doped with hydrophobic perfluorooctanesulfonate ($PFOS^-$) was superhydrophobic in its oxidized state due to the large number of PFOS anions incorporated in the polymeric matrix[64]. Thus, the hydrophobicity of ECPs can be improved by doping with hydrophobic ions.

3.2.2. *Properties*

ECPs are organic materials usually composed of C, H and heteroatoms (N, O or S) and possess unique intrinsic conductivity[63]. This intrinsic conductivity arises from their backbone consisting of the alternating single and double bonds. Hence, the delocalization of the electrons originating from the overlap of the π-bonds results in a change of the electronic and optical properties of the ECPs[68]. The polyconjugated chain has been induced with an electron deficient or rich structure by p-doping (oxidation) or n-doping (reduction), respectively[68]. To maintain the electroneutrality of the ECPs, counter ions (also called dopants) are introduced into the polymer film during the doping process[63,68]. In electrochemical doping, the ECPs are doped by applying an appropriate potential or current. The p-doping and n-doping of the ECPs doped with mobile ions are illustrated in Eq. 8 and Eq. 9, respectively, while the p-doping and n-doping of the ECPs doped with bulky ions are shown in Eq. 10 and Eq. 11, respectively.

$$ECP^0 + A^- \rightarrow ECP^+ A^- + e^- \qquad \text{p-doping with mobile anion (Eq. 8)}$$

$$ECP^0 + e^- + B^+ \rightarrow ECP^- B^+ \qquad \text{n-doping with mobile cation (Eq. 9)}$$

$$(ECP^0 R^-) B^+ \rightarrow ECP^+ R^- + e^- + B^+ \qquad \text{p-doping with immobile anion (Eq. 10)}$$

$(ECP^0\ S^+)\ A^- + e^- \rightarrow (ECP^-\ S^+) + A^-$ n-doping with immobile cation (Eq. 11)

where A^- and B^+ are the mobile anions and cations, while R^- and S^+ are the bulky anions and cations. ECP^0, ECP^+ and ECP^- are the electrically neutral, oxidized and reduced forms of the polymer, respectively. Some typical anionic dopants for ECPs are chloride (Cl^-), perchlorate (ClO_4^-), tetrafluoroborate (BF_4^-), hexafluorophosphate (PF_6^-) and polystyrene sulfonate (PSS^-)[68], while typical cationic dopants for ECPs are metal ions (such as Li^+ and Na^+[68]), tetrabutylammonium (TBA^+)[69] and tetraethylammonium (TEA^+)[68]. In the case of the bulky dopants, such as PSS^-, they are trapped in the ECP structure during synthesis. Hence, these large molecule dopants are integrated in the ECPs and will not easily leave the ECP structure during the doping process, as shown in Eq.10-11. In *paper II* and *III*, the polyazulene (PAz) was doped with hexafluorophosphate ions (PF_6^-). In *paper IV*, the hydrophobicity was introduced to the ECP film by using the hydrophobic $PFOS^-$ as the dopant. The dopant ions influence the physical and chemical properties of the ECP, such as its volume, porosity, surface morphology and hydrophobicity[68,70,71].

3.2.3. *Polarization*

The electrochemical doping process mentioned above is used to control the oxidation state of the ECP called as polarization of the ECP in this context. In order to obtain the reproducibility of E^0 of the ECP-based SC-ISEs, the ECP is recommended to be polarized at a specific oxidation or reduction potential before the drop-casting of the ISM cocktail.

The ECPs are more stable in their oxidized state and have a higher charge density compared with the neutral form. Due to the higher charge density, the conductive form is usually hydrophilic. Two methods have been reported to improve the hydrophobicity of the ECPs. It was demonstrated that switchable wettability (from hydrophobic to hydrophilic) was achieved with poly(3-alkylthiophenes) where the alkyl-substituent enhances the hydrophobicity of the ECP or by pre-polarization of the ECP in aqueous electrolyte solution[64,71-73]. In *paper II*, PAz doped with PF_6^- (PAz-PF_6) was polarized at -0.4 V (reduced form), 0.2 V (semi-oxidized form) and 1.0 V (oxidized form) to study its hydrophobicity at different oxidation potentials. It was found that the PAz-PF_6 is hydrophobic when it was polarized at $E \leq 0.2$ V. In *paper III*, the PAz-PF_6 film polarized

at 0.2 V was applied as the SC in K^+-ISEs. The polarization process improved the reproducibility and hydrophobicity of the PAz-PF_6. Moreover, in most cases, increasing the charge density of ECPs (*i.e.* their oxidation state) will increase their hydrophilicity. However, in *paper IV*, we offered a solution to this problem by obtaining the PPy that is hydrophobic in its oxidized form by incorporating the $PFOS^-$ counterions in the polymer matrix during the electropolymerization[64].

3.2.4. *Polyazulene*

Over the past few decades, synthesis and characterization of polyazulene (PAz) has attracted attention because of its electronic and optical properties[46,74-76]. The PAz films have been utilized in the supercapacitors[76], batteries[77] and electrochemical biosensors[78]. The azulene monomer is a non-alternant aromatic hydrocarbon consisting of a fused five-membered ring with a seven-membered ring. Upon the electrochemical[75,79] and chemical[80,81] polymerization, the azulene monomers are linked together at C_1 and C_3 of the five-membered ring (**Figure** 6)[82]. The electrochemically prepared PAz films possess a relatively high electrical conductivity of 10^{-2} to 1 S cm^{-1} depending on the type of the counterion[83]. Its conductivity is comparable with the polythiophene and PPy[68,83]. The electrosynthesis of the PAz film is commonly performed in organic solvent, such as acetonitrile (ACN) and dichloromethane. It was reported that the free-standing PAz films were prepared by CV in ACN, which implied that the PAz films were insoluble in ACN[84]. However, even the trace amounts of the impurities, such as water, in the organic solvent will decrease the yield of polymerization[83]. Hence, the ACN solution was stored in N_2 gas, and the electrolyte was dried under vacuum at 80 °C for 30 min prior to use. It was reported that the PAz is both p-dopable and n-dopable[85]. Although the PAz shows a stable and reversible redox behaviour in the dry electrolyte solutions, it has gained less attention than many other ECPs.

In *paper II*, it was found that the neutral form of the PAz has high hydrophobicity (water contact angle (water CA): 126±14º) due to its aromatic carbon structure. Therefore, it is expected to prevent the water layer formation when the PAz is used as the SC layer in SC-ISEs. Moreover, its areal redox capacitance (44.5 mF cm^{-2}) is three times higher than for PEDOT-PSS polymerized with the same charge density (0.5 C cm^{-2}). Hence, in *paper*

II and *III*, the PAz-PF_6^- was applied for the first time as the ion-to-electron transducer layer in the Ca^{2+}- and K^+-selective SC-ISEs. The PAz-PF_6 was synthesised with CV in ACN containing the azulene.

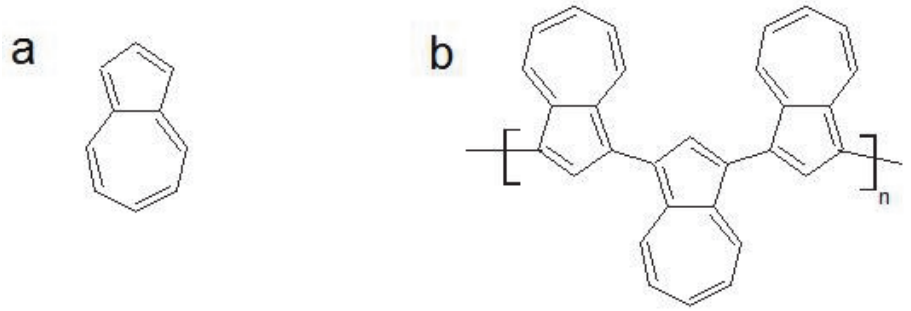

Figure 6. The chemical structures of (a) azulene and (b) PAz.

3.2.5.*Polypyrrole*

Pyrrole is a heterocyclic aromatic organic compound. Polypyrrole (PPy) is formed by the polymerization of the pyrrole monomer. The chemical structures of the pyrrole and PPy are shown in **Figure** 5 where X=NH. PPy was firstly synthesised more than 100 years ago and it is one of the most investigated ECPs. It was chemically polymerized in 1916 and electrochemically polymerized as high-quality thin films in the late 1970s[86]. The conductivities of PPy usually range from 2 to 100 S cm^{-1} depending on the electrolyte salts and solvents used for the polymerization[87]. Due to the swelling of the PPy during the charging and discharging process, it has been used as an artificial muscle[88]. Furthermore, PPy is one of the most studied and used ECP for ion sensing applications[89-91].

It was demonstrated that the surface roughness of the PPy film was increased by performing the combined electrochemical and chemical polymerization in the presence of a small amount (2.0×10^{-4} M) of $FeCl_3$[64], which increased the hydrophobicity of the PPy film to 152±2º (water CA). The Fe^{3+} functioned as an oxidant in the chemical polymerization that initiated the polymerisation process before starting the electropolymerization. In *paper IV,* PPy was synthesized at a constant current in presence of Fe^{3+} and the hydrophobic $PFOS^-$ anion was incorporated (PPy-PFOS) as the charge compensating (doping) anion from the electrolyte solution into the polymer structure.

This was expected to result in a high hydrophobicity and to prevent the aqueous layer formation beneath the ISM when PPy-PFOS was used as the SC in ISEs.

3.3. Electrically conducting polymer based potentiometric solid-contact ion-selective electrodes

The ECPs are a group of popular materials used as the SC for the potentiometric sensors. By using the ECPs as the ion-to-electron transducer, it is possible to fabricate miniaturized micropipette based electrodes[92] and microelectrodes on small planar electrode substrates[93]. Due to their oxidation and reduction reactions (Eq. 8-11) coupling the ionic and electronic conduction, the ECPs can function as the ion-to-electron transducers in SC-ISEs[4,15]. The ECP-based ion-to-electron transducer provides a well-defined interface placed between the ionically conductive ISM and the electronically conductive electrode substrate, where the ion-to-electron transfer is otherwise blocked (*i.e.* blocked interface). Hence, the selective ionic signal can be converted to a measurable electronic signal (potential) by the ECPs. The most popular ECPs applied as the SCs are based on the derivatives of PPy[91,94-96], polythiophene[97-100] or polyaniline[35,89,90,101,102]. The first ECP-based SC-ISE used PPy as the SC[53]. Poly(3-octylthiophene) (POT) and Poly(3,4-ethylenedioxythiophene) (PEDOT) belong to the derivatives of polythiophene used as SC materials. The redox capacitance of the POT under normal conditions is low, since its oxidation potential is rather high. Moreover, it shows high light sensitivity [103]hindering its use as an SC in SC-ISEs. Since polyaniline (PANI) is sensitive to protons, the PANI-based SC-ISEs are not recommended to be used for monitoring the ion concentrations in the solutions of different pH. Since PPy, PEDOT and PANI are electroactive in a broad potential range, they may react with the redox interferences and cause potential drift when used in SC-ISEs[43].

Despite the aforementioned drawbacks of ECPs as the SC in SC-ISEs, the p-doped ECPs also have many advantages and are often used as the SCs in SC-ISEs. **Figure** 7 shows the operating principle of a p-doped ECP-based K^+-selective SC-ISE[4,10].

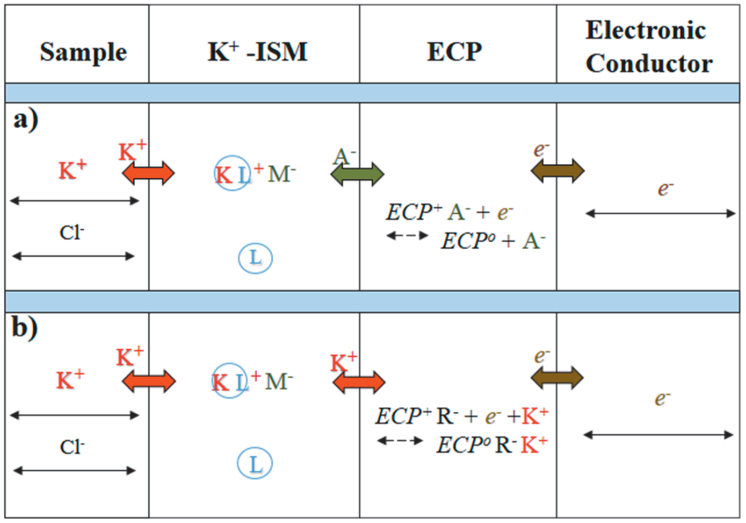

Figure 7. Operating principle of a p-doped ECP-based K^+-selective SC-ISE. The ECP is doped with anions (A^- stands for small anions and R^- stands for bulky anions). L stands for the neutral ionophores and M^- stands for the lipophilic anion in the ISM.

During the potentiometric measurements and the initial conditioning of the SC-ISEs in the analyte solution, selective complexation of analyte ions (e.g. K^+) by the ionophore occurs. Consequently, the K^+ ions transport between the ISM and the sample solution. It is followed by the ion exchange of A^- or K^+ between the ISM and the conducting polymer. The type of ion exchange at the ISM/conducting polymer interface, which is caused by the electroneutrality requirement in the ISM, depends on the mobility of the counterion incorporated in the ECP[10]. The ECPs, which are used as the ion-to-electron transducer layer in SC-ISEs, convert the ionic response of the ISM (Eq. 7) to an electronically measurable signal (potential) by the doping/de-doping (oxidation/reduction) process of the ECP.

4. Challenges in potentiometric solid-contact ion-selective electrodes

As mentioned in *Chapter* 3.1, replacing the internal solution of conventional ISEs with an SC functioning as the ion-to-electron transducer enables miniaturization of SC-ISEs [92,93]. The main challenges of ECP-based SC-ISEs are described in this chapter. The discussion is divided into two sections; problems caused by (1) the ISMs and (2) the ECP-based SCs. To fabricate ECP-based ISEs with good potential stability and reproducible standard potential (E^0) was the goal of the research work of this PhD thesis.

4.1. Challenges of plasticized PVC-based ion-selective membranes

4.1.1. *Leaching of membrane components*

PVC-based ISMs are commonly used in potentiometric ISEs and selective optodes[1,104]. Some drawbacks of PVC-based ISMs are leaching of the plasticizer[26,27], ionophore[28] and other additives[29,105] from the ISM to the solution phase influencing the response stability of ISEs. Due to the leaching process, the potential of the SC-ISEs drifts and frequent calibrations must be done in long-term use of the electrodes. The leaching of membrane components also shortens the lifetime of the ISM. Hence, the search for new polymeric membrane materials instead of PVC is important in developing robust ion sensors. These materials (with or without plasticizer) should have high hydrophobicity and the diffusion coefficients of the ion-ionophore complexes should be lower than in PVC. Hence, this prevents the ion-ionophore complexes and other membrane components to leach out from the ISM. For example, in the case of SR (with lower ion-ionophore diffusion coefficients than in plasticized PVC) and PANI-based SC-ISEs, a more stable potential response was achieved[35]. In another approach, the ionophore was covalently immobilized to the polymeric ISM to avoid the leaching of the ionophore and to reduce the transmembrane fluxes of the ions that are ionophore-mediated[106].

4.1.2. *Water uptake of ion-selective membranes*

Currently, the full prevention of the aqueous layer formation beneath the ISM, which is caused by the water uptake of ISMs, is one of the most difficult challenges[107-109]. The

water uptake of plasticized PVC-based ISMs has been previously studied by Harrison et al. in the 1990's[107,110]. It was concluded from spatial imaging photometer studies that at least two types of water were present in the ISM; 'mobile' water (miscible) and 'immobile' water (phase-separated droplets). More recently, it was shown by the FTIR-ATR spectroscopy that monomeric, dimeric, clustered and bulk water were present in the plasticized PVC-based ISMs[108,109]. In plasticized PVC-ISMs, the 'fast water', which relates to the monomeric and dimeric water, reaches the saturation level in ca. 2 h for a ca. 326 μm thick ISM, whereas the saturation time for the 'slow water' relating to the clustered and bulk water is ca. 24 h[109]. Due to the water uptake of the ISMs, a thin aqueous layer or pools of water can be formed at the electrode interfaces. When measuring solutions with high concentration of interfering ions, the interfering ions reach the inner side of the ISM facing the ECP solid contact and they are expelled to the aqueous layer/water pools due to the selectivity of ISM[15]. Hence, the aqueous layer or water pools function as electrolyte reservoirs where the primary and interfering ions may accumulate, resulting in transmembrane ion fluxes[16,111]. The composition change in this layer/pools will substantially influence the phase boundary potential between the ISM and this layer and cause potential instability[112].

The water layer can be detected by the potentiometric aqueous layer test, which was introduced by Fibbioli et al.[16]. This test is performed by recording the potential change of the SC-ISE in 0.1 M IX, 0.1 M JX and then again in 0.1 M IX solutions for at least 3-5 h in each solution (I^+, primary ion; J^+, interfering ion, X^- counter anion) for the plasticized PVC-ISMs and 24 h for the SR-ISMs[34]. The potential response of the SC-ISEs in absence of the water layer is shown as the solid line in **Figure** 8. After replacing the primary ion solution by the interfering ion solution, the potential decreases to a new stable value. When the SC-ISE is placed back in the primary ion solution, the potential returns to the initial value. In the presence of a water layer, the dotted line in **Figure** 8 presents the typical potentiometric response of the SC-ISE. After immersing the electrode in 0.1 M JX solution, the interfering J^+ ions accumulate in the water layer, while the primary I^+ ions transport through the ISM to the outer sample solution[4,16]. This compositional change of the water layer results in a rise of the electrode potential[4]. However, when the ISE is placed back into the IX solution, the replacement of J^+ by I^+ in the inner water layer takes place slowly. Consequently, the potential gradually drifts to the initial value[4,16].

The water uptake of ISMs can be reduced by decreasing the plasticizer content of the ISM or replacing the plasticized PVC-ISM with new hydrophobic ISM materials[4]. It was found that the logarithm of the diffusion coefficient of the ionophore showed a linear decrease to the increase of PVC content[106]. In another work, adding more plasticizer into the ISM increased its polarity, resulting in a higher water uptake[109]. Lindfors et al.[109] showed that the plasticizer facilitates the water uptake of ISM. Sundfors et al.[108] studied the water uptake of SR-ISMs, plasticized PVC-ISMs and poly(acrylates)-ISMs by the FTIR-ATR technique. The SR-ISM had the lowest water uptake resulting in a lower possibility of salt co-extraction and in lower ion mobility in the ISM, which is beneficial for the detection limit of the SR-based SC-ISEs[108].

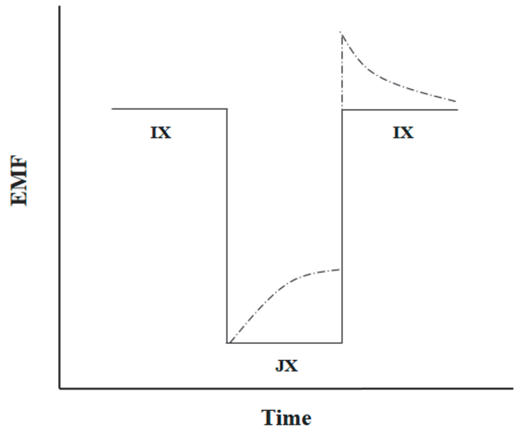

Figure 8. Schematic illustration of the potentiometric aqueous layer test. The solid and dashed lines represent SC-ISEs without and with the water layer formation, respectively.

4.2. Challenges connected to electrically conducting polymers

4.2.1. *O_2 and CO_2 sensitivity*

The O_2 and CO_2 can easily transport through the ISM and reach the surface of the ECP[43]. These molecules dissolved in the water layer or the water pools will either influence the oxidation state of the ECP (O_2) or the solution pH (CO_2). The chemical reactions of O_2 with PPy in neutral and alkaline aqueous solutions are shown as examples below[113]:

$$\frac{1}{4}O_2 + \frac{1}{2}H_2O + e^- = OH^- \quad \text{(Eq. 12)}$$

$$PPy^0 + OH^- = PPy^+(OH^-) + e^- \quad \text{(Eq. 13)}$$

Consequently, PPy^0 (non-conducting form) will be oxidized to PPy^+ (conducting form) in neutral and alkaline solutions (Eq.12-13), if the standard reduction potential of the half-cell reaction in Eq. 12 is higher than for the PPy^0/PPy^+ half-cell in Eq.13. Hence, the total cell reaction can be written as: $PPy^0 + \frac{1}{4}O_2 + \frac{1}{2}H_2O = PPy^+(OH^-)$. In acidic solutions, the oxidation and reduction reactions are expressed as:

$$\frac{1}{4}O_2 + H^+ + e^- = \frac{1}{2}H_2O \quad \text{(Eq. 14)}$$

$$PPy^0 + R^- = PPy^+(R^-) + e^- \quad \text{(Eq. 15)}$$

Their total reaction is under the same assumptions as above: $PPy^0 + \frac{1}{4}O_2 + H^+ + R^- = \frac{1}{2}H_2O + PPy^+(R^-)$, where (R^-) stands for the dopant ion. The oxidation state changes of the ECP, followed by the compensation with dopant ions, influence the phase boundary potential at the ECP/ISM interface, resulting in a potential drift of the ECP-based SC-ISEs.

In the case of CO_2, carbonic acid (H_2CO_3) is formed in water dissociating into hydrogen carbonate (HCO_3^-) and carbonate (CO_3^{2-}) ions, and protons, which alters the pH of the aqueous phase in contact with the buried ECP solid-contact[99,114]. This, in turn, may influence the potential of the ECP. PANI is one typical ECP that is pH sensitive and can therefore easily be affected by pH changes[115]. Due to its pH sensitivity, a thin layer of PANI-based optical sensor was used to measure pH between 2 and 12 in the near infrared region[116].

In *paper III* and *IV*, the O_2 and CO_2 sensitivity of the SC-ISEs were measured in 0.1 M KCl by purging it with either pure N_2, O_2 or CO_2 gas.

4.2.2. *Light sensitivity*

The light sensitivity of ECPs has been considered as one important parameter to investigate the applicability of ECPs in SC-ISEs[4,103]. Some of the ECPs have been used as photovoltaic materials, since they can convert light (photons) to electrical energy due to their suitable band gaps[63]. It was found that the PPy-FeCN and PPy-Cl films showed lower light sensitivity compared to PEDOT-PSS, POT-BF_4 and drop-cast POT[103]. Hence, it is recommended that the light sensitivity should be measured for the ECP-based SC-ISEs. In these measurements, it is important to protect the RE with an aluminum foil to eliminate the contribution of the photovoltaic effect of the Ag/AgCl wire[117]. In *papers III* and *IV*, the light sensitivity of PAz-PF_6 and PPy-PFOS was investigated by measuring the potential response of the SC-ISEs when they were exposed to darkness, ambient room light and cold light. The ambient room light was provided by a fluorescent lamp (Universal Thermo, 36 W/840). The Leica CLS 150 XE cold light source equipped with a tungsten halogen lamp (Philips EKE 150 W, 21 V) was directed towards the SC-ISEs membrane surfaces for cold light exposure.

4.3. Reproducibility and stability of solid-contact ion-selective electrodes

4.3.1. *Piece-to-piece reproducibility*

Each ECP-based SC-ISE must be calibrated before use due to the relatively large variations in the E^0 values from one SC-ISE to another. The E^0 can be obtained by extrapolating the linear part of the calibration curve to $a_{K^+} = 1$. Generally, the standard deviation (SD) of E^0 for ECP-based SC-ISEs is ca. 20 mV[93] or higher and the reproducible fabrication of calibration-free SC-ISEs is, therefore, one of the biggest challenges in the field of solid-state ISEs.

Recently, several new solid-contact approaches have been introduced. To obtain a well-defined phase boundary potential between the ISM and SC, Zou et al. applied a hydrophobic cobalt (II)/(III) 4,4'-dinonyl-2,2'-bipyridyl redox buffer complex as the SC[118]. The E^0 values with a piece-to-piece SD of 0.7 mV was reported. Zhou et al. who used tetrakis(4-chlorophenyl)borate anion doped arenethiolate protected gold nanoclusters as SC for K^+-ISEs received an SD of E^0 less than 1 mV[60]. However, the mass/industrial

production is not straightforward due to the complexity of these approaches. Adding a high-capacity redox buffer to a carbon-based SC to improve the E^0 reproducibility is another approach reported by Hu et al.[61]. In this approach, colloid-imprinted mesoporous carbon combined with lipophilic cobalt(II)/(III) tris(4,4'-dinonyl-2,2'-bipyridyl) redox buffer salt was used as the SC in K^+-selective ISEs with the SD of E^0 less than 1 mV. Besides the SC layer, the conducting electrode substrate materials can also influence the E^0 reproducibility. It was reported that the SC-ISEs prepared on Au substrates showed a better E^0 reproducibility than the identical electrodes prepared on glassy carbon substrates[59]. However, the requirements for the potential accuracy of the SC-ISEs depend on the applications. For example, for measuring Na^+ ion concentration in clinical analysis, the acceptable error is lower than ±4 mM, which corresponds to the discrepancy of E^0 less than 0.7 mV when the concentration of Na^+ was assumed to be 145 mM and the slope of the calibration curve 59.6 mV/ decade[43]. If the SC-ISEs would have good reproducibility, they could be used without calibration (*i.e.* calibration-free Na^+-ISEs).

Furthermore, it was found that the E^0 value could be adjusted by applying a potential or current[119] or by short-circuiting all the SC-ISEs at the same time in an electrolyte solution[120]. With these methods, the E^0 of the SC-ISEs is changed/shifted to a desired value due to the adjustment of the oxidation state of the ECP that determines the potential of the SC-ISE. Hence, the oxidation state of the ECPs plays an important role in the reproducibility of E^0. In *paper II*, *III* and *IV*, pre-polarization of the ECPs at a specific potential was used to stabilize (fix) the E^0 of K^+-selective SC-ISEs.

4.3.2. *Potential stability*

Conventional ISEs require frequent re-calibration due to the slow drift of their E^0. For point-of-care devices or remote environmental monitoring, ISEs that do not need frequent calibration or are calibration-free are highly demanded. These calibration-free sensors should have high piece-to-piece reproducibility and high potential stability during long-term use. Moreover, conditioning-free sensors with the potential stabilizing very quickly during the initial contact with the sample solution are preferred, because that reduces the measurement time. To achieve these goals, the potential stability of the SC-ISEs is one parameter to be considered in both short-term (*e.g.* serum analysis) and long-term

applications (*e.g.* remote measurements). The reasons for the potential drifts of the SC-ISEs have been discussed in *Chapters* 4.2 and 4.3.

In 2002, it was reported that redox-active self-assembled monolayers were used as SC for ISEs to improve the potential stability[58]. However, the ratio of the redox couples was difficult to control and their redox buffer capacity was comparatively small[43,58] . The potential drift of the SC-ISEs can also be decreased from 320±60 to 70±20 μV h^{-1} by incorporating lipophilic Ag-ligand complexes into the ISM[55]. In another work, the tetrakis(4-chlorophenyl)borate doped Au nanocluster based K^+-ISEs showed a very low potential drift of 10.1±0.3 μV h^{-1} during 72 h in 0.1 M KCl[60]. However, the most stable SC-ISEs reported are the electrodes using colloid-imprinted mesoporous carbon as SC, which had an EMF drift of only 1.3±0.3 μV h^{-1} (n=3) during 70 h in 1 mM KCl (measured under temperature control)[61]. This might be ascribed to the high double layer capacitance of the mesoporous carbon-based SC. Furthermore, it was found that the SC-ISEs prepared on Au and glassy carbon substrates had shorter equilibration time than those prepared on Pt substrates, when the electrodes were exposed to the sample solution for the first time[121].

In *papers II - IV*, a new approach was introduced to improve the E^0 reproducibility of K^+-selective SC-ISEs. It is based on pre-polarization of the PAz-PF_6 and PPy-PFOS SCs at a specific potential before depositing the ISM on top of them. The equilibrium potential of the pure PAz-PF_6 and PPy-PFOS SCs in 0.1 M KCl solution was chosen as the pre-polarization potential. The aim of the pre-polarization of the SC was also to shorten the conditioning time of SC-ISEs. Without the pre-polarization of ECPs, it can be speculated that the conditioning time for newly made SC-ISEs is in the range of a few hours to a few days, which may depend on the diffusion coefficient of water and ions in the ISMs and the relaxation time of ECPs. With the pre-polarization, the potential of SC-ISEs reached a stable state after 1 h during their first contact with unstirred 0.1 M KCl solution.

The main goal of this thesis work is to improve the potential reproducibility and stability of ECP-based SC-ISEs. The methods used focus on utilization of hydrophobic materials, especially the hydrophobic SC materials. The hydrophobic PAz was used as the SC layer and hydrophobization of ECP layer by pre-polarization and doping with hydrophobic perfluorinated anions were used to reduce the effect of detrimental water layer formed beneath the ISM.

5. Main characterization techniques

In this chapter, the main characterization techniques used in *paper I-IV* are listed and briefly introduced. The water amount in ISMs was determined by oven-based coulometric KF titrations. The water uptake of ISMs and ECP films was monitored by the FTIR-ATR technique. CV was used for both the electropolymerization and characterization of the conjugated polymers and the performance of the ISEs was tested by potentiometry. Furthermore, water CA measurements were used to determine the hydrophobicity of ECP films.

5.1. Oven-based coulometric Karl Fischer titration

The KF titration technique which was developed by Karl Fischer in 1935 is a classical method for the assessment of trace levels of water (ppm) in liquid or solid samples[122]. Today, the KF titrator equipped with an oven evaporation compartment is usually used for the water determination in solid samples[123]. The conventional titration solution is a methanolic solution that contains iodide, sulfur dioxide and a base (imidazole) as the buffer. The cathodic and anodic electrodes are called generator electrodes. During the conditioning or the titration, iodine gas is electrochemically generated at the anode, as illustrated in **Figure** 9. At the cathode, the H^+ ions are reduced to H_2. Besides this electrochemical cell, the potential of the double pin platinum electrode is monitored during the titration by passing a constant current between the pins. The titration reaction contains three steps:

$$\text{I: } 2\ I^- \rightarrow I_2 + 2e^- \qquad \text{(Eq. 16)}$$

$$\text{II: } 2\ [RNH] + 2e^- \rightarrow H_2 + 2\ RN^- \qquad \text{(Eq. 17)}$$

$$\text{III: } H_2O + I_2 + SO_2 + CH_3OH + 3\ RN^- \rightarrow [RNH]SO_4CH_3 + 2[RNH]I \qquad \text{(Eq. 18)}$$

where RN^- stands for the imidazole base. According to these equations, the molar ratio of H_2O and I_2 is 1:1 by stoichiometry. In other words, two electrons are consumed for each mole of I_2 and H_2O. H_2O carried by the N_2 gas comes from the solid sample (*i.e.* ISM) that is placed in the oven compartment. As long as there is water, no free iodine will exist in the titration solution, according to Eq. 18. A small and constant current is applied to the

double pin platinum electrode. At the equivalence point, excess iodine gas, which is caused by the absent reaction with H_2O, results in a decreased potential between the double Pt pin electrodes. Hence, this bipotentiometric end-point detection of the titration is marked by a sharp voltage drop detected by the double Pt electrode.

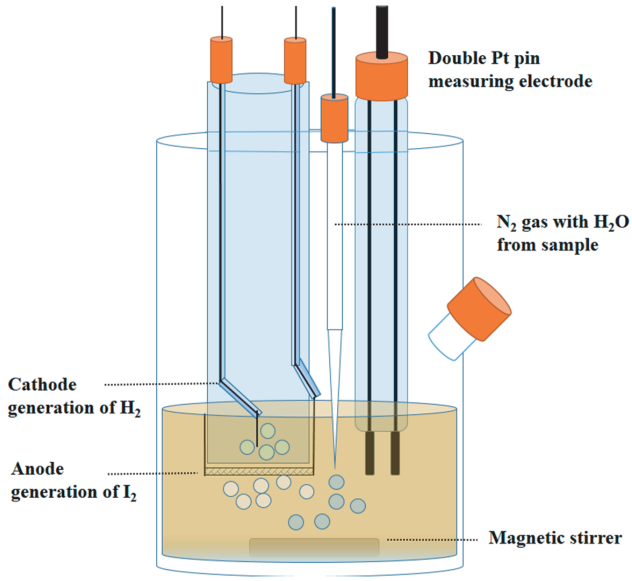

Figure 9. Schematic figure of coulometric Karl Fischer titrator.

The water uptake was studied with the oven-based coulometric KF technique for the plasticized PVC or SR (RTV 3140) matrices and for the full Ca^{2+}-selective ISM formulation in *paper I*.

5.2. *In situ* Fourier transform infrared attenuated total reflection spectroscopy

Infrared (IR) spectroscopy measures the ability of the bonds in a molecule to absorb IR radiation. This absorption increases the vibrational energy of the bonds and occurs at a wavelength which is specific for each functional group in a molecule. The vibrational frequency is dependent on the rigidity of the bond, the mass of the atoms in the bond and the surrounding of the the molecule. Higher dipole moment displacements in the bond

between two atoms in a molecule results in higher intensity of the IR absorption. Fundamental vibrations of molecules can be observed in the mid-IR region in the wavenumber range of approximately 400-4000 cm^{-1} [124,125]. *In situ* IR spectroscopy is a powerful technique to measure water uptake of ISMs. As shown in **Figure** 10, the OH stretching vibrations are visible in the wavenumber range 2950-3800 cm^{-1}, which was used for interpretation of the water uptake of ISMs and ECPs in this thesis[125,126]. Furthermore, triple bonds and double bonds can be found in the range of 2015-2270 and 1500-1860 cm^{-1}, respectively[126].

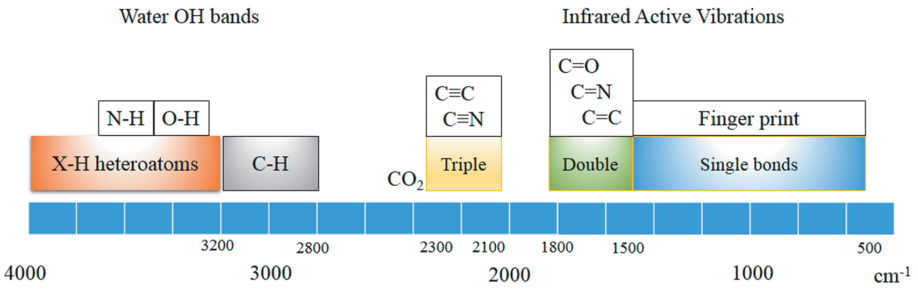

Figure 10. IR absorption wavenumber regions of different types of bands..

Two IR reflection techniques have been used for the *in situ* characterization of ECPs: external and internal reflection[124]. The incident IR beam hits the sample from its backside in internal reflection and not from the surface as in external reflection. In the internal reflection technique, an internal reflection element (IRE) with a high refractive index is used to direct the infrared radiation towards the sample which is tightly attached/pressed against the IRE[124]. However, in the external reflection technique, the IR beam passes through an IR transparent window and electrolyte solution, and reaches the surface of the polymer[127]. The internal reflection technique was used in this thesis to study water uptake of the hydrophobic SC materials and ISMs and to characterize the changes in the SCs due to polarization.

In order to obtain total internal reflection, the IRE must have a higher refractive index (n) than the sample, *i.e.* the incident beam approaches an optically less dense medium from an optically denser medium. In this thesis, a zinc selenide (ZnSe) crystal was used as the

IRE with a refractive index n=2.43-2.44 in the wavenumber range 2950-3800 cm^{-1} used for the water uptake determination. ZnSe was especially suitable due to its electrochemical stability and IR transparency in a wide wavenumber range 500-20000 cm^{-1}. Another requirement for total reflection is that the angle of incidence by which the IR radiation enters the sample is greater than the critical angle (θ_c) which can be estimated from Snell's law (Eq. 19)[128].

$$\theta_c = \sin^{-1} \frac{n_{sample}}{n_{IRE}} \qquad \text{(Eq. 19)}$$

For instance, assuming n_{sample} equals to 1.5, which is a typical refractive index value for organic compounds, θ_c becomes 43° in case of ZnSe[128]. At the reflection point between the IRE and the sample, the electromagnetic field perpendicular to the IR beam forms an evanescent wave, which propagates into the sample and decays exponentially from the surface of the IRE, as shown in the figure at the right side of **Figure** 11. The evanescent wave becomes gradually attenuated due to absorption by the sample that gives the name attenuated total reflection (ATR) for the technique. The effective penetration depth (d_p), which is defined as the distance in which the electrical field has decayed to 1/e of its initial amplitude is wavelength dependent and is given by the Harrick equation[128]:

$$d_p = \frac{\lambda}{2\pi\, n_{IRE} \sqrt{\sin^2\theta - \left(\frac{n_{sample}}{n_{IRE}}\right)^2}} \qquad \text{(Eq. 20)}$$

where λ is the wavelength of the radiation and θ is the angle of the incident beam. For example, when λ = 10 μm (i.e. wavenumber of 1000 cm^{-1}), n_{IRE} = 2.43 (ZnSe), n_{sample} =1.5, and θ = 45°, the approximate depth of penetration is 1.9 μm[128].

By combining infrared spectroscopy and electrochemistry, i.e. *in situ* spectroelectrochemistry, the spectral changes at different redox states of ECPs coated on the surface of the IRE can be observed. The infrared active vibration (IRAV) bands (wavenumber below 1800 cm^{-1}) are commonly used as the characteristic fingerprint for ECPs and is considered as the specific range for monitoring the doping reaction of ECPs[127]. The increasing number of charged groups on the ECP chain when it is oxidized from neutral to conductive form increases the dipole moment of specific vibrations, and

results in a strong increase in the absorption intensity of those IR bands[127]. Moreover, during the conversion of ECPs into the conducting form, electronic absorbance occurs and a broad absorption band becomes visible at the high-energy end of the mid-IR region (from ~1700-7000 cm^{-1}).

The schematic drawing of the *in situ* spectroelectrochemical FTIR-ATR cell is shown in **Figure** 11. The ZnSe crystal coated with a thin sputtered layer of Pt (15 or 30 nm) was used as the working electrode (WE) for the electrochemical polymerization or potentiometric measurement of PAz and PPy and their SC-ISEs (*paper II* and *IV*). A Pt disc and an Ag/AgCl electrode served as counter and reference electrodes, respectively. In *paper I*, a three-electrode electrochemical cell was not used, since only the water uptake of ISMs was measured and a bare ZnSe crystal was used as the IR waveguide in a similar cell construction.

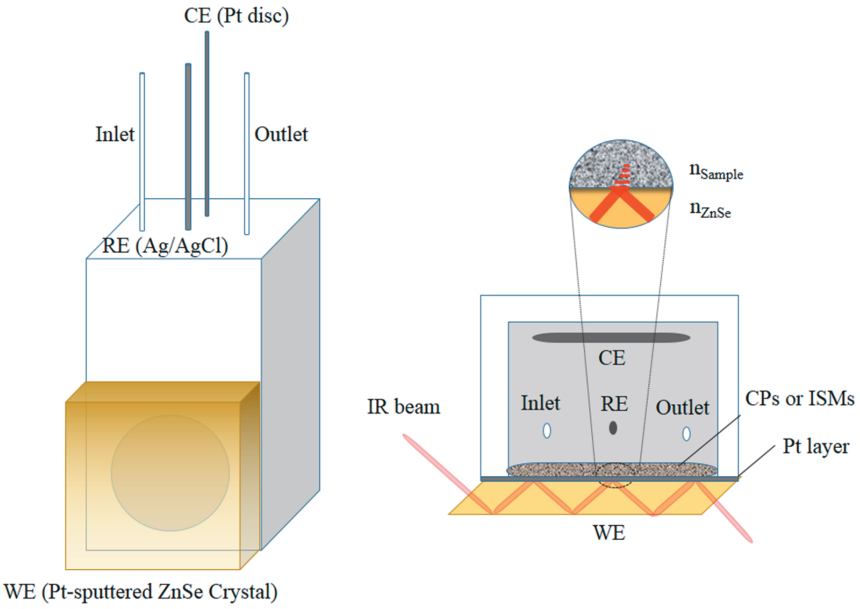

Figure 11. Left: schematic view of the *in situ* spectroelectrochemical FTIR-ATR cell. Right: top view of the cell.

5.3. Cyclic voltammetry

In cyclic voltammetry (CV), a linearly changing potential is applied on the working electrode, *i.e.* the potential is scanned back and forth between two potential limits. The current is recorded and plotted against the applied potential, resulting in a cyclic voltammogram. In the case of ECPs, CV can be used as an electropolymerization technique in monomer-containing electrolyte solution and as a characterization technique to study the redox process of ECPs during their doping in the monomer-free electrolyte solution.

In the case of CV used for the electropolymerization of ECPs, an oxidation peak of the monomer becomes visible at the high potential end of each potential scan. At successive cycles during oxidative polymerization, CV shows an oxidation peak due to the growing polymer film starts to become visible at a lower potential than the monomer oxidation when the potential is cycled from low to high potential and a reduction peak when the potential is cycled in the opposite way. Moreover, CV is the most common technique to interpret the mechanism of the oxidation and reduction processes and can be used to characterize the redox processes of ECPs. The total charge involved in the charging and discharging process of an ECP can be obtained by integrating the area of the CV. During the oxidation and reduction of ECPs, there will be the electron transfer at the electrode | polymer interface, and simultaneously transfer of dopant ions across the polymer | electrolyte solution interface to balance the charge of the polymer backbone. In the case of a very thin film, the oxidation and reduction peaks are fully reversible. In that case, oxidation and reduction peak currents are proportional to the scan rate. In the case of thicker films, where the dopant ions have a limited mobility, the doping is a diffusion-controlled process. The peak current is then proportional to the square-root of the scan rate[129,130]. Typically, the scan rate is in the range of 20 mV/s to 100 mV/s. Due to the slow transfer of dopant ions and/or the structural changes of the polymer film during its doping/de-doping process, a large hysteresis (anodic and cathodic peak separation) is generally observed[65].

The CV experiments were done in a three-electrode electrochemical cell, which consists of a RE, WE and CE (also known as an auxiliary electrode). The Ag/AgCl wire, which is made by coating an Ag wire with AgCl, was used as the RE in both organic and aqueous

media. The materials for the working electrode used in this work include Pt-sputtered ITO glass, Pt coated ZnSe and glassy carbon. The potential is controlled between WE and RE. CE can be any material that conducts current easily and is inert in the sample solution. Typically, a coiled platinum wire, which provides a much larger surface area than that of the working electrode, is used as the counter electrode and the current generated between CE and WE is monitored.

In *paper II* and *III*, CV was used to synthesize and characterize the PAz-PF_6 film. The integrated charge was used to determine the degradation of the ECP film in contact with the aqueous solution.

5.4. Water contact angle measurements

The most common way to determine the wettability and hydrophobicity of a polymer film is by measuring the water CA. It is defined as the angle between the liquid-vapour interface and the liquid-solid interface. The Young equation describes the relationship between the interfacial tensions and the water CA for the ideal case[131]. In the case when the liquids completely fill the voids at a rough surface, the Wenzel equation interprets the correlation between the apparent (θ_A) and the Young contact angle (θ_Y) [132]:

$$\cos\theta_A = r\cos\theta_Y \qquad \text{(Eq. 21)}$$

where r, the roughness ratio, is defined as the ratio between the actual and the apparent surface. According to this equation, the surface roughness will enhance both the hydrophobicity ($\theta_Y > 90\,°$) and the hydrophilicity ($\theta_Y < 90\,°$). In this thesis, the static water CA was measured 10 s after adding a drop of water onto the ECP surface by the sessile drop method. This technique was used in *paper II* and *IV* to determine the water CA of the PAz-PF_6 and PPy-PFOS, respectively.

5.5. Potentiometry

Potentiometry is a relatively cost-effective and simple method from the instrumentation point of view. In potentiometry the equilibrium potential difference (*i.e.* EMF) is measured between a RE and an indicator electrode in the sample solution, which has been discussed in *Chapter* 2.3. The EMF is the sum of the potential drops at the phase

boundaries and also inside the phases. In the case of ISEs, their potential is in proportion to the logarithm of the analyte activity in the presence of interfering ions based on the Nikolskii-Eisenman equation (see *Chapter* 2). This relationship relies on the boundary potential at the interface of the ISM and sample solution, which requires that the other boundary potentials are constant. Potentiometry is a zero-current method, because a negligible current is applied to the electrochemical cell. In *paper II*, *III* and *IV*, potentiometry has been used to characterize the performance of the SC-ISEs. The EMF was measured by a 16-channel potentiometer (input impedance: 10^{15} Ω, Lawson Lab, Inc.). The potential stability, selectivity, working range, sensitivity, reproducibility and life time of ISEs can be described and compared with the potentiometric measurements. Moreover, a salt bridge was used for the RE to avoid the leaching and contamination of the sample solution by KCl. In the case of an Ag/AgCl wire as the inner reference electrode, aluminum foil was used to cover RE to avoid the photovoltaic effect of Ag when studying the light sensitivity of the SC-ISEs.

6. Results and discussion

This chapter describes the main results and discussion. *Chapter* 6.1 focuses on the water uptake measurements of ISMs (*paper I*). *Chapter* 6.2 is about the properties of PAz and its application as the SC layer for ISEs (*paper II* and *III*). *Chapter* 6.3 describes the properties of PPy-PFOS and its application as the SC layer for ISEs (*paper IV*). The electrode substrate used for SEM and water CA measurements was metallized ITO, while glassy carbon electrodes were used for the basic characterization of the SC-ISEs and Pt-sputtered ZnSe elements for FTIR-ATR measurements of ECPs and their ISEs.

6.1. Water uptake of ion-selective membranes

In *paper I*, the water uptake of plasticized PVC- and SR-ISMs was quantified with the oven-based coulometric KF technique. Five different ISM types were studied:

- Plasticized PVC matrix (PVC:DOS (1:2))
- SR matrix (only RTV 3140)
- CaISM(IV-PVC): 98.75 wt% PVC:DOS (1:2), 0.45 wt% KTFPB, and 0.8 wt% calcium ionophore IV
- CaISM(I-PVC): 98.75 wt% PVC:DOS (1:2), 0.45 wt% KTFPB, and 0.8 wt% calcium ionophore I
- CaISM(I-SR): 98.1 wt% RTV 3140, 0.9 wt% KTFPB, and 1.0 wt% calcium ionophore I.

These five different types of ISMs were contacted either symmetrically from both sides or asymmetrically from one side with deionized water (DIW) or 0.1 M $CaCl_2$, KCl or NaCl solutions for 24 h, and their water uptake was determined by the KF technique. In the FTIR-ATR setup, the membranes were in contact with aqueous solution from one side to mimic the asymmetrical measurements by the KF technique. The water content at the ISM | ZnSe interface was monitored by the FTIR-ATR setup and compared with that determined by the KF technique. The water content in freshly prepared SR membranes (SR matrix and CaISM(I-SR)) that had not been in contact with any aqueous solutions was 2-4 times higher than in all plasticized PVC ISEs determined by the KF technique. It

was speculated that the lower water uptake of the SR membranes after being in contact with water was due to the saturated state of its initial water content. Interestingly, it was found that there was a transmembrane flux of water (uptake/release) when the ISMs were immersed in different electrolyte solutions. To the best of my knowledge, this has not been previously reported. The transmembrane flux of water may influence the potential response of the ISM-based SC-ISEs besides the flux of primary and interfering ions.

6.1.1. Oven-based coulometric Karl Fischer titrations

Symmetrical contact. As shown in **Table** 1, in the case of plasticized PVC-based membranes, their water uptake is lower in 0.1 M solutions of $CaCl_2$, NaCl and KCl than in DIW due to the lower osmotic pressure of those solutions. The water uptake of the plasticized PVC matrix is about half of the CaISM(IV-PVC) and CaISM(I-PVC) membranes. It is because the KTFPB, ETH5234 and ETH1001 in the Ca^{2+}-selective ISMs have ionic or polar groups that increase the hydrophilicity and polarity of the ISMs. The water uptake of Ca-ISM(IV-PVC) in DIW is slightly lower than for Ca-ISM(I-PVC), which is ascribed rather to higher lipophilicity of calcium ionophore IV than calcium ionophore I. This indicates that lipophilic ISM components decrease the water uptake of the ISM and consequently may reduce the potential drift of the SC-ISEs. The highest water uptake (1660 ± 370 ppm) of plasticized PVC membranes was obtained by the Ca-ISM(I-PVC) in DIW. A similar water uptake of the ISMs symmetrically contacted with the 0.1 M $CaCl_2$, NaCl and KCl electrolyte solutions was obtained for the PVC matrix and Ca-ISM(I-PVC). The relative SD values for the individual measurements were 4-36% for PVC membranes and 4-41% for the SR membranes, as published in the Supporting Information in *paper I*. It is reasonable to have relatively high SD values due to the low sample mass (ca. 0.15 g).

As shown in **Table** 1, for the SR-based membranes, their water uptake is much lower than for the plasticized PVC-based membranes, which is in good accordance with the published results obtained by the FTIR-ATR technique[108]. However, the SR-based membranes initially contain more water than the PVC membranes, probably due to the moisture cured RTV 3140 formulation used as the SR matrix material. Water is incorporated in SR, since the curing of RTV 3140 occurs by absorbing a small amount of moisture from air. The water content of as-prepared SR membranes is 1030±20 ppm for

the SR matrix and 1500±320 for the Ca-ISM(I-SR), whereas the water content of as-prepared PVC membranes is 610±20 ppm for the PVC matrix, 420±30 ppm for the Ca-ISM(IV-PVC) and 670±90 ppm for the Ca-ISM(I-PVC). The higher water content of as-prepared SR membranes results in lower water uptake when they are in contact with aqueous solutions, due to the lower osmotic pressure compared with the less water containing plasticized PVC-based membranes. Similar water uptake of membranes symmetrically contacted with 0.1 M $CaCl_2$, NaCl and KCl electrolyte solution was determined for the SR matrix and Ca-ISM(I-SR).

Table 1. The water uptake of PVC and SR membranes symmetrically contacted for 24 h with DIW and 0.1 M solutions of $CaCl_2$, NaCl and KCl (n=3)[133].

Membrane type	***DIW***	***0.1 M $CaCl_2$***	***0.1 M NaCl***	***0.1 M KCl***
PVC matrix	700 ± 230	470 ± 220	480 ± 230	460 ± 230
Ca-ISM(IV-PVC)	1470 ± 710	970 ± 450	930 ± 15	830 ± 460
Ca-ISM(I-PVC)	1660 ± 370	850 ± 410	Not measured	Not measured
SR matrix	190 ± 80	290 ± 50	220 ± 100	220 ± 50
Ca-ISM(I-SR)	310 ± 500	350 ± 380	210 ± 540	Not measured

Asymmetrical contact. The water uptake of PVC and SR membranes asymmetrically contacted for 24 h with DIW and 0.1 M $CaCl_2$ solution is shown in **Table** 2. The asymmetrical contacting mimics the water uptake process in the FTIR-ATR setup, where only one side of the ISM faces the aqueous solution. The water uptake of the ISM in the asymmetrical contact mode is much lower than that in symmetrical one. Although the standard deviations are very high, it is found that the water uptake in DIW is higher than in 0.1 M $CaCl_2$ for both PVC- and SR-based membranes. However, no clear difference of water uptake is found for the PVC matrix and Ca-ISM(IV-PVC) due to their low water uptake and the relatively high SDs.

To conclude, the oven-based coulometric KF titration provides a way to quantify the water uptake of the ISMs. However, this technique is not able to monitor the low water

uptake of the ISMs having low sample weight, especially in the case of SR-based membranes and their asymmetrical contact with water. Since the detection limit of oven-based coulometric KF titration is 10 µg-200 mg, and the sample weight of membranes is ca. 0.15 g, the water uptake which can be measured must be higher than 67 ppm.

Table 2. The water uptake of PVC and SR membranes asymmetrically contacted for 24 h with DIW and 0.1 M $CaCl_2$ (n=3)[133].

Membrane type	***DIW***	***0.1 M $CaCl_2$***
PVC matrix	220±300	80±90
Ca-ISM(IV-PVC)	240±210	30±60
SR matrix	90±70	150±70
Ca-ISM(I-SR)	180±170	200±170

6.1.2. Fourier transform infrared spectroscopy-attenuated total reflection measurements

The water uptake obtained by the oven-based coulometric KF method was verified with the FTIR-ATR technique. Both the positive and negative water bands indicate the water uptake increase and decrease, respectively, at the interface of the ISM and the ZnSe element. The OH stretching band in the wavenumber region of 2950-3750 cm^{-1} (strong vibrations) was chosen for monitoring the water uptake. However, additional water bands can be found in the spectra at <1000 cm^{-1}, 1640-1645 cm^{-1} (OH bending vibrations)[126], and ~2125 cm^{-1} (broad peak)[109]. It was proved that the FTIR-ATR technique can detect traces of water, so the FTIR-ATR technique is more sensitive than the oven-based coulometric KF method[133].

Plasticized PVC-based ISMs. The water uptake of Ca-ISM(IV-PVC) (thickness: 95 µm) was continuously measured in DIW and 0.1 $CaCl_2$ for 96 h. The spectra are shown in **Figure** 12. The ISM was first in contact with DIW for 48 h (**Figure** 12a, b) to allow the membrane to be fully equilibrated (hydrated) in water. After 2 h the water uptake

almost reached the equilibrium, since from 2 to 24 h only a minor increase of water uptake was observed. A new background was always taken to re-zero the IR spectrum before the sample solution was changed according to the specific sequence. As a result, the first spectrum achieved is identical with a straight line. The positive or negative bands indicate the increase or decrease of water uptake, respectively. **Figure** 12b (t=24-48h) shows that no obvious change of water bands was observed, indicating that the water uptake of the ISM was fully equilibrated. In **Figure** 12c (t=48-72h), negative bands were found after replacing DIW with 0.1 M $CaCl_2$, showing that the transmembrane flux of water occurred due to the lower osmotic pressure of 0.1 M $CaCl_2$. This decrease of water uptake is in good accordance with the lower water uptake of PVC-based ISMs measured in 0.1 M $CaCl_2$ compared to DIW, as shown in **Table** 1 and 2 by the coulometric KF measurements. Moreover, the transmembrane flux of water from the ISM to the solution phase after replacing 0.1 M $CaCl_2$ with deionized water was slow and did not reach an equilibrium in 24 h, which may result in a long-term potential instability of SC-ISEs partially due to the interference of the water molecules. In **Figure** 12d (t=72-96h), the 0.1 M $CaCl_2$ solution was replaced by DIW to increase the osmotic pressure of the sample solution. An increasing O-H stretching band indicates an opposite transmembrane flux of water between the electrolyte solution and ISM. The maximum absorbance in **Figure** 12d was only 0.003 A.U., which indicated that the water uptake of Ca-ISM(IV-PVC) could not fully be recovered, since the minimum absorbance of the water uptake in **Figure** 12c was 0.125 A.U. The spectra in **Figure** 12 clearly show the influence of the electrolyte solution on the water uptake of the PVC-ISM. This transmembrane flux of water will induce interference at the SC and probably influence the interfacial potentials at the ISM/SC and SC/electrode substrate interfaces) resulting in a potential drift of the SC-ISEs.

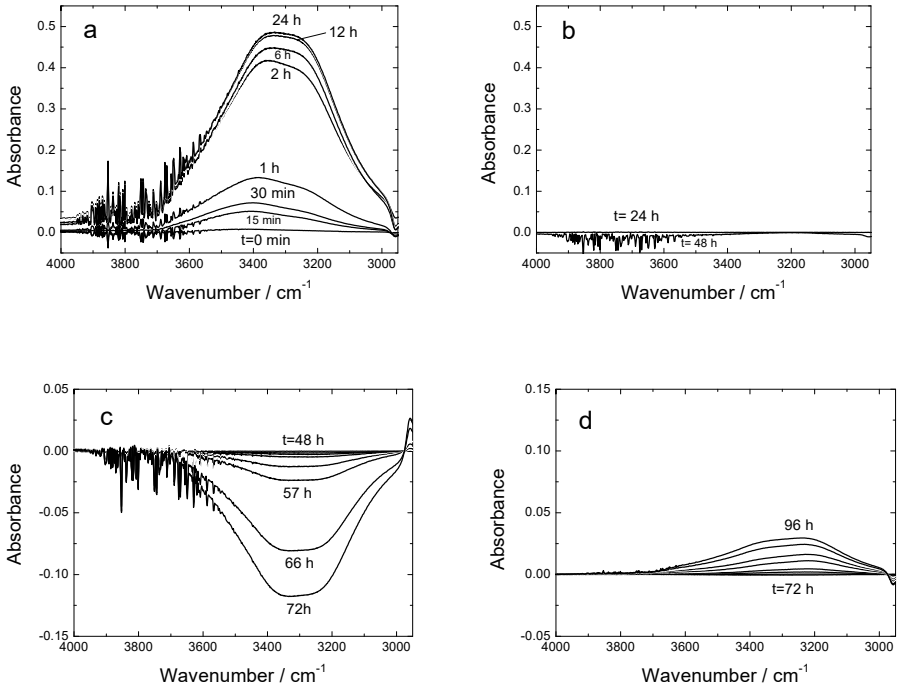

Figure 12. FTIR-ATR spectra of the Ca-ISM(IV-PVC) membrane (thickness: 95 µm) continuously contacted for 96 h in the following sequence with: (a, b) DIW (0-48 h), (c) 0.1 M $CaCl_2$ (48-72 h) and (d) DIW (72-96 h)[133].

Silicone rubber-based ISMs. The Ca-ISM(I-SR) (thickness: 118 µm) was exposed to DIW and 0.1 M $CaCl_2$ in the same order as the Ca-ISM(IV-PVC). The spectrum in **Figure** 13a (0-24 h), shows that the water uptake of Ca-ISM(I-SR) in DIW (maximum absorbance: 0.08) was much lower than for Ca-ISM(IV-PVC) (maximum absorbance: 0.48). In **Figure** 13b (24-48 h), after re-zeroing of the spectrum at 24 h, the maximum absorbance slowly increased to 0.02 A.U., indicating that the water diffusion is slower in SR than in plasticized PVC-ISMs where the water uptake equilibrium in plasticized PVC-based membranes was reached in ca. 2 h, as shown in **Figure** 12a. A negative and positive peak change of the OH-stretching bands was found in **Figure** 13c and 13d for Ca-ISM(I-SR), respectively, indicating the influence of electrolyte solution on the water uptake of Ca-ISM(I-SR).

Although the FTIR-ATR technique is not a quantitative method, it is a more powerful technique compared with the oven-based coulometric KF technique in monitoring the transmembrane flux of water in ISMs placed in contact with different electrolyte solutions. Moreover, the water uptake measured with this technique can be used for mathematical modelling of the water diffusion coefficients in the ISM and SC[134,135].

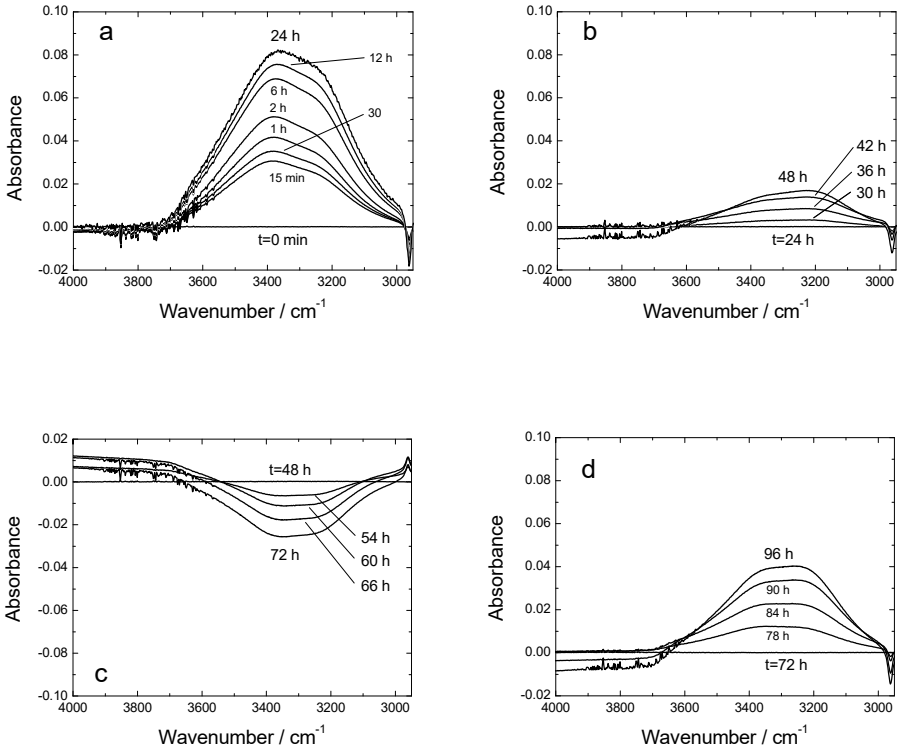

Figure 13. FTIR-ATR spectra of the Ca-ISM(I-SR) (thickness: 118 μm) continuously contacted for 96 h in the following sequence with: (a, b) DIW (0-48 h), (c) 0.1 M $CaCl_2$ (48-72 h) and (d) DIW (72-96 h)[133].

6.2. Polyazulene based solid-contact ion-selective electrodes

The electrosynthesized PAz was introduced for the first time as the ion-to-electron transducer layer for SC-ISEs. It was shown that the semiconducting form of PAz possesses relatively high hydrophobicity (water CA: 98±11º) due to its aromatic carbon structure. Moreover, its redox capacitance is three times higher than for PEDOT-PSS (prepared with the same polymerization charge). These two advantages make PAz attractive as a new SC material in SC-ISEs. In *paper II*, the hydrophobicity of PAz films by modifying their oxidation states was identified by water CA measurement. The hydrophobic form of PAz was used for the fabrication of SC-ISEs to reduce the water uptake of the SC. Furthermore, the electrochemical stability of PAz was studied in 0.1 M $CaCl_2$ solution to determine its equilibrium potential in direct contact with aqueous solution. The influence of the pre-polarization of PAz at three different potentials (-0.4 V, 0.2 V and 1.0 V) on the potential stability of PAz-based Ca^{2+}-selective SC-ISEs was also investigated in this paper. In *paper III,* the pre-polarization of PAz (before the drop casting of the cocktail solution on top of it) was introduced to improve the reproducibility of E^0 of PAz-based SC-ISEs[103]. The EMF stability was studied in the absence of O_2 and CO_2 and the water layer formation was investigated by the potentiometric aqueous layer test.

6.2.1. Characterization of polyazulene

The PAz film was synthesized on Pt sputtered ITO glass for SEM and the water CA measurements, and on GC substrates incorporated in polyether ether ketone (PEEK) bodies for the SC-ISEs fabrication. The polymerization of PAz was performed by cycling the potential between -0.6 V and 1.2 V. The CVs of PAz-PF_6 polymerized with different number of cycles were measured in monomer-free solution and indicated that the electroactivity, charge (integrated area of CVs) and capacitance of the films increased by the number of potential cycles, as shown in the discussion below.

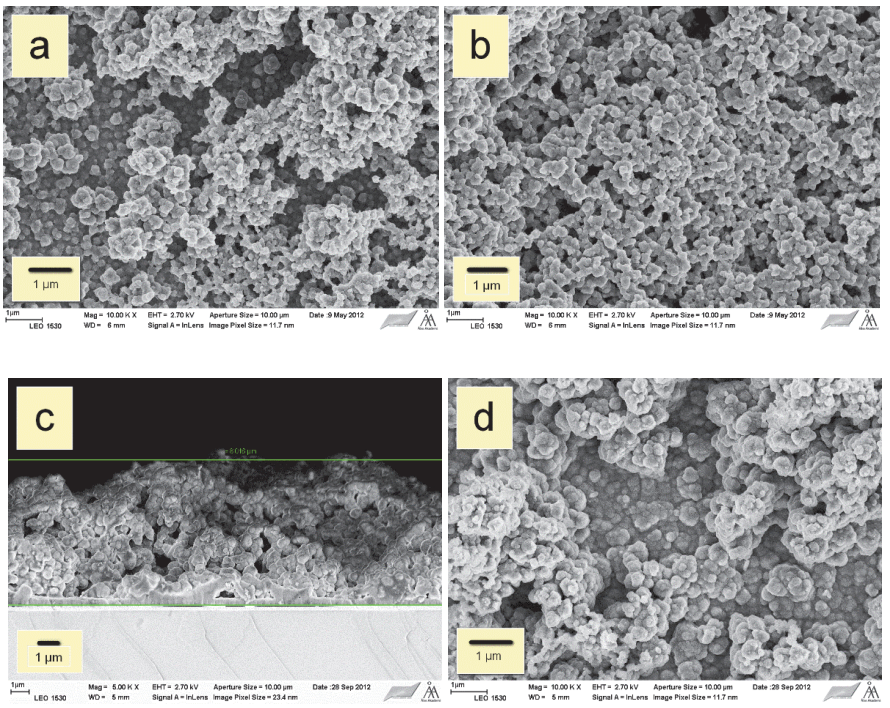

Figure 14. SEM images of PAz films electropolymerized on ITO without rinsing: **(a)** 5 and **(b)** 25 potential cycles. Films polymerized with rinsing for 10 cycles: **(c)** cross section and **(d)** surface image. Magnification: 10000 x; (c): 5000 x [136].

As shown in **Figure** 14, the PAz films have an open surface morphology. The PAz film polymerized with 25 cycles (**Figure** 14b) has a more compact structure than films prepared with 5 cycles (**Figure** 14a). To obtain a less porous and denser film, as shown in **Figure** 14c and 14d, the PAz films were rinsed by ethanol after every second polymerization cycle with the aim of washing out the oligomers from the film surface and obtain a denser film. Using the PAz film as the SC layer, a compact film helps to prevent water to reach the electrode substrate and to form an aqueous layer, which results in transmembrane ion fluxes to the SC | electrode substrate interface. However, a more porous film may give a better adhesion (larger contact area) to the ion-selective membrane.

After the polymerization, the water CAs of pre-polarized PAz films at E = -0.4 V prepared with 5, 10 and 25 cycles were 82±17º, 126±14º, and 122±8º, respectively, indicating that nearly superhydrophobic films could be prepared with 10 and 25

polymerization cycles. The water CAs of the PAz films prepared with 25 cycles and polarized at -0.4 V and 1.0 V are shown in **Figure** 15a and 15b, respectively. Similar to polyaniline and poly(3-hexylthiophene)[137], the PAz film in the conducting form (pre-polarized at 1.0 V) is more hydrophilic than in the neutral form (pre-polarized at -0.4 V). The water CA of the PAz film at the semi-conducting form (pre-polarized at 0.2 V) is 98±11º, which is still rather hydrophobic. The hydrophobicity of the PAz film (pre-polarized at E ≤ 0.2 V) probably contributes to the prevention of the aqueous layer formation at the SC | electrode substrate interface.

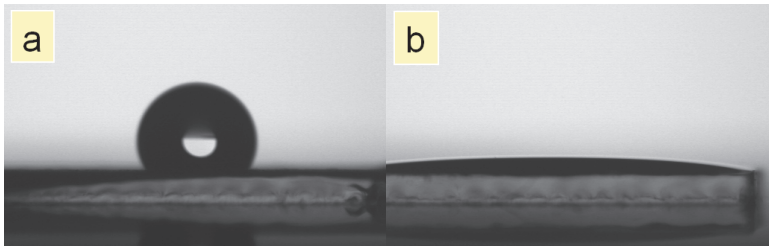

Figure 15. Water droplets during contact angle measurements on top of PAz films polarized at: **(a)** -0.4 V and **(b)** 1.0 V [136]. The PAz film was electropolymerized with 25 potential cycles by rinsing the film surface after every second cycle.

Furthermore, the redox capacitance of the PAz films (conducting form) was measured by electrochemical impedance spectroscopy. It has been pointed out that a sufficiently high capacitance of the solid contact is a prerequisite to obtain stable SC-ISEs potentials[138]. The redox capacitance of the PAz films polymerized with different number of cycles was determined from the low frequency range (10-100 mHz) of impedance spectrum. It was 28 mF cm^{-2} for PAz film polymerized with 5 cycles, 62 mF cm^{-2} for 10 cycles and 109 mF cm^{-2} for 25 cycles. Furthermore, the PAz films were polymerized at 0.93 V to the charge of 0.5 C cm^{-2}, to compare their redox capacitance with other ECPs with the same charge density[45]. The redox capacitance of the PAz film (45 mF cm^{-2}) is three times higher than the PEDOT-PSS film (15 mF cm^{-2})[45], but lower than for the composite film of PANI and graphene oxide (77 mF cm^{-2})[102]. The relatively high redox buffer capacitance of PAz-PF_6 is expected to improve the long-term potential stability of PAz-PF_6 based SC-ISEs.

6.2.2. Influence of pre-polarization of polyazulene on potential stability

The influence of pre-polarization[103] of the PAz films on the potential stability of Ca^{2+}-selective SC-ISEs was measured when the electrodes were in initial contact with aqueous solution. As shown in **Figure** 16, three Ca^{2+}-selective SC-ISEs based on the PAz films pre-polarized at -0.4 V, 0.2 V and 1.0 V and one Ca^{2+}-selective CWE were tested. The highest potential drift (4.0 mV h^{-1} during 24 h) was observed for the CWE, due to the ill-defined interface between the ISM and the electrode substrate. The most stable SC-ISEs are the ones with the PAz film pre-polarized at -0.4 V and 0.2 V, which is in good accordance with the high hydrophobicity of the PAz film in its semiconducting and reduced forms. The potential drift is only 0.5 mV h^{-1} for both of them during the measurement time of 24 h. The potentials of these two electrodes stabilized in less than 4 h, whereas the one with PAz pre-polarized at 1.0 V had the longest stabilization time of ca. 14 h. Hence, not only the potential drift was lowered, but also the stabilization time was shortened by the pre-polarization. Moreover, the pre-polarization of PAz film shifted the EMF of the SC-ISEs. A higher potential applied during the pre-polarization can shift the EMF of the SC-ISEs to higher values and vice versa. As shown in **Figure** 16, the electrode with the PAz film pre-polarized at 1.0 V had the highest EMF, while the electrode with the PAz film pre-polarized at -0.4 V had the lowest EMF, since the oxidation state change of the SC by pre-polarization changed the E^0 of the SC-ISEs. Vanamo et al. showed that the EMF and E^0 of PEDOT based SC-ISEs could be shifted by applying a constant potential or current pulses to the SC-ISEs, *i.e.* after coating the SC with the ISM[119]. In this case, the doping level of the SC layer was adjusted with the ion transportation between ISM and SC and ion transport through the ISM. However, the tuned E^0 gradually drifted back towards the initial E^0, which was ascribed to the spontaneous redox reaction of the SC[43,119]. After comparing these two methods, it is concluded that the pre-polarization of SC layer tunes the EMF of SC-ISEs to a more stable state. It might also shorten the conditioning time and increase the reproducibility of E^0. A combination of these two methods may be beneficial.

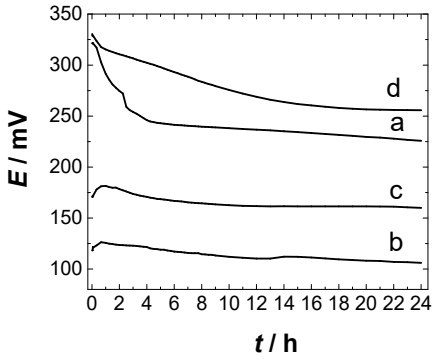

Figure 16. The potential stability of the Ca^{2+}-selective CWE and the PAz-based SC-ISEs in 0.1 M $CaCl_2$ solution. The CWE (a) and the SC-ISEs which were pre-polarized at (b) -0.4 V, (c) 0.2 V and (d) 1.0 V. The Ca^{2+}-ISMs had the following thicknesses: CWE, 115 µm; SC-ISE (-0.4/0.2/1.0 V), 118/111/118 µm[136].

6.2.3. Application of hydrophobic polyazulene in potassium solid-contact ion-selective electrodes

Prior to the K^+-ISM deposition, the PAz film was polarized at 0.2 V for 5 min in 0.1 M monomer-free solution. As shown in **Figure** 16, the best electrodes are the ones based on the PAz film pre-polarized at 0.2 V and -0.4 V. The PAz film polarized at 0.2 V is partially conductive, whereas it is nonconductive or less conductive when it is polarized at -0.4 V. To keep the hydrophobicity and conductivity of the SC, 0.2 V was selected as the pre-polarization potential.

To show the advantage of the hydrophobic PAz film as the SC, the potential response of the PAz-based K^+-selective SC-ISEs was compared with the commonly used chemically synthesised POT-based SC-ISEs due to their similar water CA[72]. The water CA of the PAz film polarized at 0.2 V was 98±11º while POT was ca. 110º. **Figure** 17 shows the superior performance of the PAz-based SC-ISEs during their initial contact with a 10^{-3} M KCl solution over the POT-based SC-ISEs. The SD of EMF is calculated based on four identical electrodes of each type. Between 2 min to 1 h, the mean EMF drifts calculated for the PAz and POT-based SC-ISEs were 0.65 and 2.3 mV h^{-1}, respectively. After 1 h to 12 h, the EMF drift of the PAz-based electrodes was 0.67 mV h^{-1}, whereas in the case of

the POT-based electrodes, it decreased to 0.95 mV h^{-1}. However, the EMF drift for the PAz-based SC-ISEs between 12 h and 49.5 h was only 29 μV h^{-1}, while the drift for the POT-based electrodes was still 0.5 mV h^{-1}. The SD of EMF for the PAz-based electrodes reached 3.1 mV at 2 min, whereas for POT, it was 11.2 mV. Interestingly, the SD for PAz-based electrodes was below 3.5 mV after 49.5 h but for the POT-based counterpart, it increased in time and reached the maximum value of 20.9 mV. The results suggest that the initial potential of the pre-polarized PAz-based K^+-selective SC-ISEs stabilized in one hour and had a potential drift below 0.67 mV h^{-1}, indicating that they could be used without long-term conditioning. However, the SD of EMF for the PAz-based electrodes is not low enough for calibration-free applications.

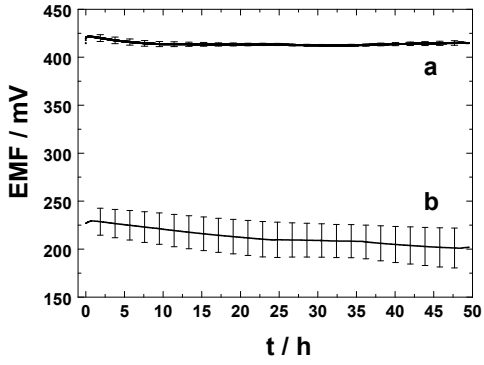

Figure 17. Potential response of the (a) PAz- and (b) POT-based K^+-selective SC-ISEs (n=4) at their first contact (after fabrication) with a 10^{-3} M KCl solution[139].

The PAz-based K^+-selective SC-ISEs (n=4) were calibrated in 10^{-3}-10^{-9} M KCl solutions. The potential trace curve was measured from high to low concentrations in KCl solution, as shown in **Figure** 18a. The inset plot in **Figure** 18a shows the potential trace of the electrodes when the solution was diluted from $10^{-6.5}$ to 10^{-7} M KCl solution and the corresponding calibration curve is plotted in **Figure** 18b. The slope of the calibration curve (*i.e.* the sensitivity of the electrodes) calculated from its linear part (10^{-6}-10^{-2} M) was close to Nernstian with a slope of 57.0±0.3 mV/decade (r^2 = 0.9999). The SD of the E^0 was ±7.9 mV, which indicates that the PAz-based K^+-selective SC-ISEs are still not good enough without calibration at least for K^+ detection in clinical applications[43]. The LDL of the electrodes was (7.2±0.9)×10^{-8} M. After conditioning in 10^{-4} M KCl solution,

the selectivity coefficients of the SC-ISEs were determined in 0.1 M solutions of KCl, $MgCl_2$, LiCl, NaCl, NH_4Cl and $CaCl_2$, giving the following selectivity coefficients: $logK^{pot}_{K^+,Mg^{2+}}$= -4.0±0.1, $logK^{pot}_{K^+,Li^+}$= -5.0±0.1, $logK^{pot}_{K^+,Na^+}$= -4.3±0.1, $logK^{pot}_{K^+,NH_4^+}$= -4.3±0.1 and $logK^{pot}_{K^+,Ca^{2+}}$= -4.0±0.1, which are in good accordance with the published selectivity coefficients for the valinomycin-based ISEs[140].

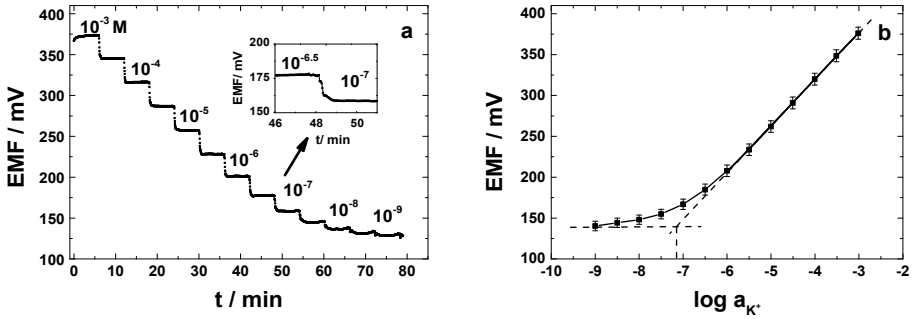

Figure 18. PAz-based SC-ISEs: (a) The potential trace curve measured when the K^+-concentration is successively lowered and (b) the calibration graph (*n*=3). Inset in (a): expansion of the selected concentration range[139].

The potentiometric aqueous layer test for the PAz-based SC-ISEs and the CWEs is shown in **Figure** 19. The lack of potential drifts for the PAz-based SC-ISEs indicates that no water layer is formed. An instant potential change of ca. 208 mV was observed when the solution was changed from 0.1 M KCl to 0.1 M NaCl, which reflects the selectivity of K^+ to Na^+. The potential drift after changing the electrolyte solution from 0.1 M NaCl back to 0.1 M KCl, is only 0.1 mV h^{-1}, which exhibits a remarkable electrode stability. This low potential drift could be caused by the relatively high redox capacitance of the PAz film (conducting form) and the absence of water layer at the ISM/SC interface. In contrast to the good potential stability of the SC-ISEs, the CWEs show a typical potential drift for ISEs with a water layer formation at the interface of the ISM and SC. Generally, due to the high water uptake of the plasticized PVC-ISMs, the presence of a water layer in SC-ISEs based on plasticized PVC and ECPs is very common. In summary, PAz works successfully as a water barrier underneath the ISM, which shows that PAz is a good choice as the SC material for the SC-ISEs.

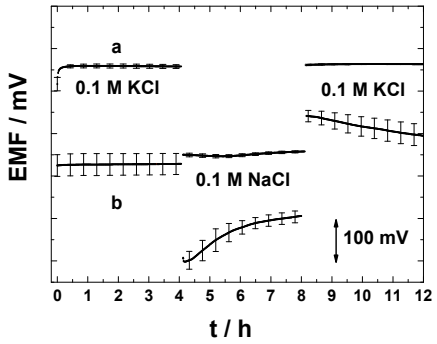

Figure 19. Potentiometric aqueous layer test for the K^+-selective (a) PAz-based SC-ISEs and (b) the CWEs. After t=4 h, the electrolyte solution was changed from the primary ion (K^+) to the interfering ion (Na^+) solution and was replaced again with the primary ion solution at t=8 h (n=3)[139].

The sensitivities to O_2 and CO_2 of the pre-polarized PAz-based SC-ISE were studied by purging the relevant gas to the 0.1 M KCl solution. After each step, N_2 was purged to remove the residual gases. At the same time, the potentials of the PAz-based electrodes were monitored. As shown in **Figure** 20a, the EMF increased only 1 mV during 1 h when purging O_2 through the solution. In addition, no significant effect from CO_2 on the SC-ISEs was found. Hence, at the normal measurement conditions, the effect from O_2 and CO_2 was negligible for the PAz-based SC-ISEs.

As illustrated in **Figure** 20b, the light sensitivity of the SC-ISEs was measured in dark conditions, under ambient room light and intensive cold light. No obvious potential drift was found when the light source was changed between the dark conditions and the ambient room light. In the worst case, upon exposure of the electrodes to intensive direct cold light, the EMF drift was less than 0.5 mV during 30 min, indicating that the PAz-based SC-ISEs have no light sensitivity under normal illumination conditions. In the case of pure POT films (without the ISM), the potential drift was reported to be more than 300 mV when changing the illumination condition from dark to cold light[103]. Hence, the PAz-based SC-ISE has an excellent potential stability to light being superior to the POT-based SC-ISEs.

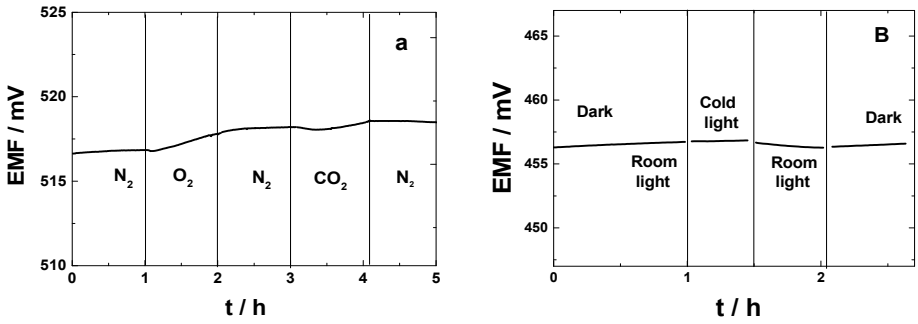

Figure 20. (a) Sensitivity to O_2 and CO_2 and (b) light sensitivity of the PAz-based K^+-selective SC-ISEs measured in 0.1 M KCl[139].

6.3. Hydrophobic polypyrrole based solid-contact ion-selective electrodes

In general, ECPs are hydrophilic when their charge density in their oxidized form is increased. In the application of ECPs as SC for SC-ISEs, the high hydrophobicity and conductivity of ECP is required to obtain a stable potential for the electrodes. Nevertheless, in *paper IV*, we offered a solution to the problem that the ECPs are hydrophobic in their oxidized form by using a highly hydrophobic doping anion in the film formation of PPy. The proof of this concept is shown by the application of the PPy film doped with $PFOS^-$ as the SC in K^+-selective SC-ISEs.

6.3.1. Characterization of hydrophobic polypyrrole

The CVs of PPy-PFOS measured in 0.05 M TEAPFOS-ACN solution show that PPy-PFOS converts to the oxidized form already at E > ca. -0.6 V, which is typical for PPy prepared with a bulky immobile anion such as dodecylsulphate[141]. The doping process of ECPs with bulky immobile anions was discussed in *Chapter* 3.3. For PPy-PFOS, TEA^+ is the main charge compensating ion in the doping/dedoping of the film during CVs and polarization. The obtained SEM images of the PPy-PFOS film shown in **Figure** 21 reveal that the film has a relatively compact morphology, compared with the PAz-PF_6 film shown in **Figure** 14. The thickness of PPy-PFOS is ca. 1.4 µm measured from the cross section of the film by SEM. The water CA of the PPy-PFOS films polarized for 10 min at

-0.4 V and 0.2 V was 67±17º and 97±5º (*n*=3), respectively. This shows that the films are more hydrophobic in their conducting form, contrary to PAz-PF_6 and the other ECPs. This phenomenon indicates that the higher pre-polarization potential facilitates the incorporation of more $PFOS^-$ anions into the PPy matrix, resulting in a higher hydrophobicity.

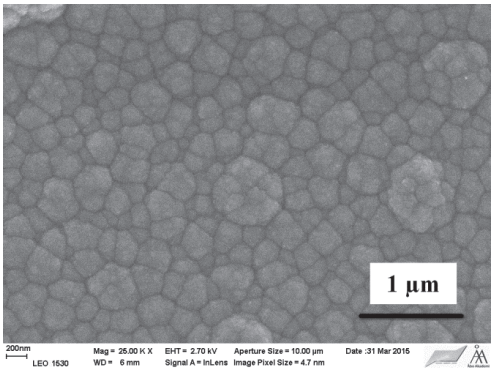

Figure 21. The SEM surface image of the PPy-PFOS film electropolymerized on ITO and pre-polarized at 0.18 V for 10 min. Magnification: 25000×[135].

6.3.2. Water uptake of hydrophobic polypyrrole

The water uptake of the bare PPy-PFOS film pre-polarized at 0.18 V was studied with the FTIR-ATR spectroscopy. This simulates the extreme situation when the SC is directly exposed to water. However, as a buried layer beneath the ISM, the SC is exposed to only very minor amounts of water (ca. 50-500 ppm, *i.e.* the water content in plasticized PVC membranes)[133]. As shown in **Figure** 22, the gradually increasing OH-stretching bands from water (ca. 2960-3750 cm^{-1})[108,109,111,112,142] reveal that its water uptake is very slow. The penetration depth of the IR beam calculated in *Chapter* 5.2 is lower than ca. 0.7 µm in this wavenumber region. Because of the absence of OH-stretching bands in the FTIR-ATR spectrum for the spectra measured at t=1 min, it is believed that the evanescent field of the IR beam penetrates only into the PPy film in this wavenumber region. This is different from the PAz film in which the evanescent IR beam penetrated through the more porous PAz film and was, therefore, in contact with water already in the very beginning of the measurements. The mathematical simulations[108,109] of the water diffusion coefficients in PPy-PFOS were done based on the integrated absorbance of the OH-

stretching bands at 2720-4060 cm^{-1}. They show that the water diffusion in the PPy-PFOS film could be described with a model consisting of two diffusion coefficients: $D_1=9\times10^{-13}$ cm^2 s^{-1} and $D_2=2\times10^{-14}$ cm^2 s^{-1}. These diffusion coefficients reveal that the water diffuses slowly through the PPy-PFOS film that will prevent the water layer formation at the interface between SC and electrode substrate. In **Figure** 22, the band at 1128 cm^{-1} assigned to asymmetric SO_3 stretching vibration in $PFOS^-$ decreased[126], revealing that some of the $PFOS^-$ leaves the film due to the concentration gradient of $PFOS^-$ between the PPy film and DIW. The transfer of $PFOS^-$ might cause the change of the oxidation state and hydrophobicity of the PPy film. However, in the case of PPy-PFOS as SC in SC-ISEs, only a minor amount of water will be in direct contact with the PPy film, since it is buried beneath the protective ISM. Therefore, the majority of $PFOS^-$ ions should stay in the PPy film giving the film its hydrophobicity. However, over a long period of time, it is speculated that the oxidation state of the PPy film might change and some $PFOS^-$ ions might transport into the water that has penetrated through the ISM to the SC | ISM interface. As a result, the potential of the SC-ISE is expected to drift.

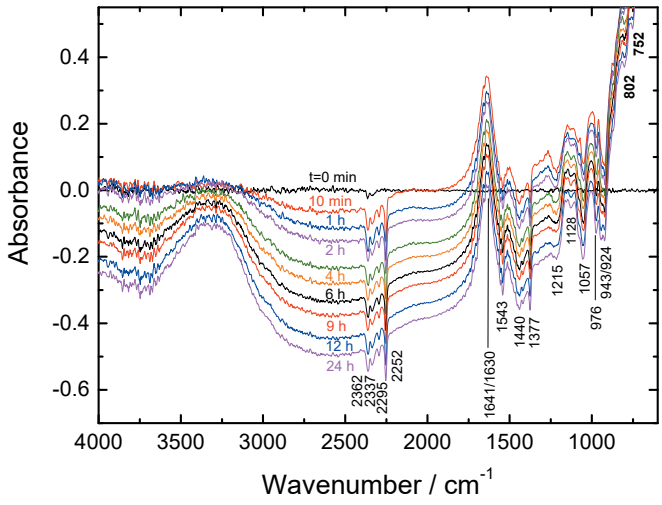

Figure 22. The FTIR-ATR spectra measured during the water uptake of the neat PPy-PFOS film in DIW during 24 h[135].

6.3.3. Hydrophobic polypyrrole applied in potassium solid-contact ion-selective electrodes

The pre-polarization of the SCs at 0.18 V carried out in direct contact with the primary ion solution, might be beneficial in achieving much shorter conditioning times[134]. It was found that the K^+-SC-ISEs reached a stable potential after 1 h from their very first contact with unstirred aqueous 0.1 M KCl solution. After stabilization of the potential during the first hour, the SC-ISEs showed a relatively low potential drift of -71 μV h^{-1} for the next 15 h at room temperature (23±2°C). As shown in **Figure** 23a, the staircase-shaped potential traces indicate that the electrodes have a fast response to the concentration changes. The electrodes had a close to Nernstian slope of 57.0±0.1 mV/decade (r^2=0.999) and a LOD of (8.8±2.1)×10^{-8} M calculated from **Figure** 23b. Most remarkably, the K^+-SC-ISEs possessed in the best case an excellent E^0 reproducibility of 501.0±0.7 mV (n=4), which is the same as has been previously reported for redox buffer based SCs purposely tuned for calibration-free applications (SD of 0.7 mV)[118] and surpasses all state-of-the-art ECP-based SC-ISEs that usually have SDs of ±20 mV[93]. The improved E^0 reproducibility of the K^+-SC-ISEs can be ascribed to the combination of the pre-polarization and high hydrophobicity of the PPy-PFOS, which stabilizes the oxidation state of the SC before the ISM casting and hinders the detrimental aqueous layer/pool formation beneath the ISM during the measurement.

The PPy-PFOS based K^+-SC-ISEs showed neither CO_2 nor light sensitivity, and nearly no sensitivity to O_2 (only 1.5 mV when changing from the oxygen-free to air saturated solution) in 0.1 M KCl solution. This shows further that the hydrophobic PPy-PFOS is suitable as ion-to-electron transducer for SC-ISEs.

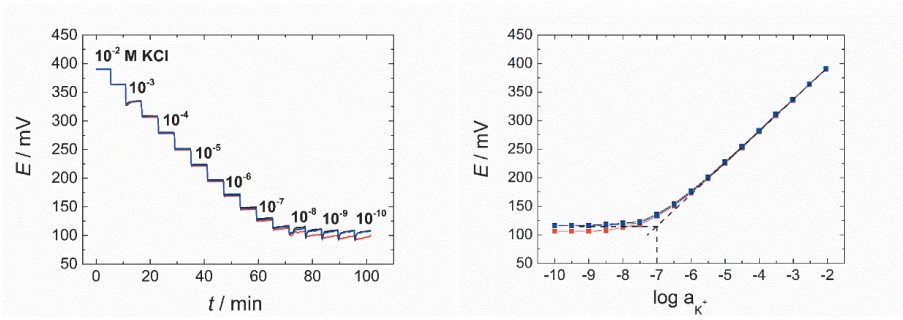

Figure 23. (a). Potential traces and (b) calibration graphs of three identically prepared PPy-PFOS based K^+-SC-ISEs (*n*=3). The dashed lines in (b) illustrate the determination of the LOD[135].

Due to the high water uptake of plasticized PVC-based ISMs, it is always a challenge to avoid the water layer formation beneath the ISMs[111]. Remarkably, as shown in **Figure** 24, no indications of an aqueous layer formation were found from the potentiometric water layer test due to the lack of drifts when changing the sample solution between the highly concentrated primary (K^+) and interfering ion (Na^+) solutions. This indicates that the hydrophobic PPy-PFOS functions as a water barrier. The absence of aqueous layer formation has been previously reported only in a few cases for ECP-based SC-ISEs, such as the K^+-selective electrodes with hydrophobic PAz[139], PPy doped with hexacyanoferrate (II)/(III) (PPy-FeCN)[93] and Ca^{2+}-selective ISEs with chemically prepared POT as the SC[143]. Moreover, in the energy dispersive X-ray spectra at 2.3 keV[144], sulphur could be detected neither on the top side of the freshly prepared ISM facing towards the solution nor on the bottom side facing the SC (not contacted with water). This reveals that the bulky $PFOS^-$ ions stay in the PPy film during the electrode preparation making it hydrophobic.

Moreover, as shown in **Figure** 24, the potential differences of the SC-ISEs in 0.1 M KCl before and after the exposure to 0.1 M NaCl solution are ca. 1.7±0.4 mV (*n*=3), which shows that the K^+-SC-ISEs have good potential stability. The absence of the aqueous layer formation in **Figure** 24 indicates the oxidization state of the PPy-PFOS SC does not change beneath the ISM. The PPy-PFOS film functions thus successfully as a water barrier, which is in good accordance with the low water diffusion coefficients calculated by the mathematical modeling of the FTIR-ATR spectra.

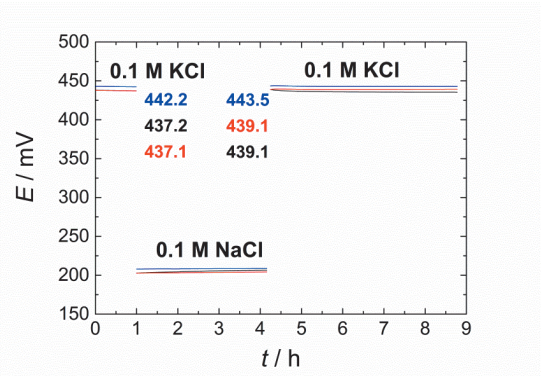

Figure 24. Potentiometric aqueous layer test for the PPy-PFOS based K^+-SC-ISEs (n=3)[135].

7. Conclusions

The piece-to-piece reproducibility and potential stability of SC-ISEs are two parameters challenging the ISE community. The research carried out in this PhD thesis mainly focused on the water uptake of the ISMs, hydrophobicity of the SC materials and their influence on the performance of SC-ISEs.

In *paper I*, the water uptake of the plasticized PVC and SR-based ISMs was quantified with the oven-based coulometric KF technique and compared with the FTIR-ATR spectra measured *in situ* during the water uptake. It was found that the water content in SR-based membrane was initially 2-4 times higher than in the PVC-based ISMs. Interestingly, the FTIR-ATR measurements confirmed that for both the PVC and SR-based ISMs the water uptake, *i.e.* water reaching the ZnSe substrate/ISM interface, was influenced by the composition of the electrolyte solution. It reveals that the transmembrane flux of water occurs. Due to the low water uptake and sample mass, the FTIR-ATR technique provided more reliable results than the coulometric oven-based KF technique, especially for the SR-based ISMs.

In *paper II* and *III*, PAz has been introduced for the first time as the ion-to-electron transducer in SC-ISEs. The water CA measurements show that PAz can be made hydrophobic (98±11º) by polarization at E=0.2 V (semiconducting form). The pre-polarized PAz-based K^+-SC-ISEs showed that the E^0 variation in the worst case was ±7.9 mV (n=4). In the view of E^0 reproducibility, the SC-ISEs based on carbonaceous materials incorporating redox buffers had better E^0 reproducibility[118], but the simplicity of the pre-polarized PAz-based K^+-selective SC-ISEs fabrication can compensate this minor deficiency in many applications. There is no evidence for the water layer formation beneath the plasticized PVC-based ISM for the PAz-based SC-ISEs and insignificant sensitivity to light, O_2 and CO_2. This makes PAz a robust alternative to the state of the art SCs used in SC-ISEs.

In *paper IV*, for the first time, PPy doped with hydrophobic $PFOS^-$ anions was used as the ion-to-electron transducer in SC-ISEs. In the best case, a superior E^0 reproducibility of 501.0±0.7 mV (n=4) was obtained. This is attributed to the combination of the pre-

polarization of the PPy-PFOS and its high hydrophobicity in the conducting form (water CA= 97 ±5º). A mathematical model consisting of two diffusion coefficients showed that the diffusion of water through the PPy-PFOS was very slow and was best described by $D_1 = 9\times10^{-13}$ cm^2 s^{-1} and $D_2 = 2\times10^{-14}$ cm^2 s^{-1}. It indicates that the pre-polarized PPy-PFOS film functions as an excellent water barrier, which is in good accordance with the potentiometric aqueous layer test.

In summary, the PhD thesis shows that the water uptake of ISMs and SCs can be studied with the FTIR-ATR and the oven-based coulometric KF titration techniques. It shows that the composition of the sample solutions significantly influences the water uptake of ISM. It is also shown that pre-polarization and hydrophobization of the SC with hydrophobic perfluorinated dopant ions improved the properties of ECP-based SC-ISEs - especially the E^0 reproducibility - and prevented the water layer formation. In the best case, the E^0 deviation was 0.7 mV, which is the smallest value reported up to now for ECP-based SC-ISEs.

8. References

(1) Bakker, E.; Bühlmann, P.; Pretsch, E. *Chem. Rev.* **1997**, *97*, 3083-3132.

(2) Bühlmann, P.; Pretsch, E.; Bakker, E. *Chem. Rev.* **1998**, *98*, 1593-1688.

(3) Bakker, E. *Anal. Chem.* **2004**, *76*, 3285-3298.

(4) Mikhelson, K. N. *Ion-selective electrodes*; Springer: Heidelberg, 2013.

(5) Gyurcsányi, R. E.; Vigassy, T.; Pretsch, E. *Chem. Commun.* **2003**, 2560-2561.

(6) Chumbimuni-Torres, K. Y.; Dai, Z.; Rubinova, N.; Xiang, Y.; Pretsch, E.; Wang, J.; Bakker, E. *J. Am. Chem. Soc.* **2006**, *128*, 13676-13677.

(7) Ding, J.; Lei, J.; Ma, X.; Gong, J.; Qin, W. *Anal. Chem.* **2014**, *86*, 9412-9416.

(8) Szűcs, J.; Gyurcsányi, R. E. *Electroanalysis* **2012**, *24*, 146-152.

(9) Lan, W. J.; Zou, X. U.; Hamedi, M. M.; Hu, J.; Parolo, C.; Maxwell, E. J.; Bühlmann, P.; Whitesides, G. M. *Anal. Chem.* **2014**, *86*, 9548-9553.

(10) Hu, J.; Ho, K. T.; Zou, X. U.; Smyrl, W. H.; Stein, A.; Bühlmann, P. *Anal. Chem.* **2015**, *87*, 2981-2987.

(11) Bandodkar, A. J.; Hung, V. W. S.; Jia, W.; Valdes-Ramirez, G.; Windmiller, J. R.; Martinez, A. G.; Ramirez, J.; Chan, G.; Kerman, K.; Wang, J. *Analyst* **2013**, *138*, 123-128.

(12) Gao, W.; Emaminejad, S.; Nyein, H. Y. Y.; Challa, S.; Chen, K.; Peck, A.; Fahad, H. M.; Ota, H.; Shiraki, H.; Kiriya, D.; Lien, D.-H.; Brooks, G. A.; Davis, R. W.; Javey, A. *Nature* **2016**, *529*, 509-514.

(13) Bakker, E.; Bühlmann, P.; Pretsch, E. *Talanta* **2004**, *63*, 3-20.

(14) Burnett, R. W.; Covington, A. K.; Fogh-Andersen, N.; Külpmann Wolf, R.; Lewenstam, A.; Maas, A. H. J.; Müller-Plathe, O.; Sachs, C.; Siggaard-Andersen, O.; VanKessel, A. L.; Zijlstra, W. G. In *Clinical Chemistry and Laboratory Medicine*, 2000, p 1065.

(15) Bobacka, J.; Ivaska, A.; Lewenstam, A. *Chem. Rev.* **2008**, *108*, 329-351.

(16) Fibbioli, M.; Morf, W. E.; Badertscher, M.; De Rooij, N. F.; Pretsch, E. *Electroanalysis* **2000**, *12*, 1286-1292.

(17) Wang, J. *Analytical electrochemistry*; Wiley: Hoboken, 2006.

(18) Lindner, E.; Gyurcsányi, R. E. *J. Solid State Electrochem.* **2009**, *13*, 51-68.

(19) Cattrall, R. W.; Freiser, H. *Anal. Chem.* **1971**, *43*, 1905-1906.

(20) Nikolskii, B. P.; Materova, E. A. In *Ion-Selective Electrode Reviews*, Thomas, J. D. R., Ed.; Elsevier, 1985, pp 3-39.

(21) Bakker, E.; Willer, M.; Lerchi, M.; Seiler, K.; Pretsch, E. *Anal. Chem.* **1994**, *66*, 516-521.

(22) Janata, J. i. *Principles of chemical sensors*; Plenum: New York, 1989.

(23) Armstrong, R. D.; Horvai, G. *Electrochim. Acta.* **1990**, *35*, 1-7.

(24) Bühlmann, P.; Chen, L. D. In *Supramolecular Chemistry*; John Wiley & Sons, Ltd, 2012, pp 2539-2579.

(25) Hofmeister, F. *Arch. Exp. Pathol. Pharmakol* **1888**, *24*, 247-260.

(26) Reinhoudt, D. N.; Engbersen, J. F. J.; Brzozka, Z.; Van der Vlekkert, H. H.; Honig, G. W. N.; Holterman, H. A. J.; Verkerk, U. H. *Anal. Chem.* **1994**, *66*, 3618-3623.

(27) De Marco, R.; Veder, J.-P.; Clarke, G.; Nelson, A.; Prince, K.; Pretsch, E.; Bakker, E. *Phys. Chem. Chem. Phys.* **2008**, *10*, 73-76.

(28) Dinten, O.; Spichiger, U. E.; Chaniotakis, N.; Gehrig, P.; Rusterholz, B.; Morf, W. E.; Simon, W. *Anal. Chem.* **1991**, *63*, 596-603.

(29) Oesch, U.; Simon, W. *Anal. Chem.* **1980**, *52*, 692-700.

(30) Li, X. Z.; Petrovic, S.; Harrison, D. J. *Sens. Actuators, B* **1990**, *1*, 275-280.

(31) Li, X.; Harrison, D. J. *Anal. Chem.* **1991**, *63*, 2168-2174.

(32) Oh, B. K.; Kim, C. Y.; Lee, H. J.; Rho, K. L.; Cha, G. S.; Nam, H. *Anal. Chem.* **1996**, *68*, 503-508.

(33) Poplawski, M. E.; Brown, R. B.; Rho, K. L.; Yun, S. Y.; Lee, H. J.; Cha, G. S.; Paeng, K.-J. *Anal. Chim. Acta* **1997**, *355*, 249-257.

(34) Boeva, Z. A.; Lindfors, T. *Sens. Actuators, B* **2016**, *224*, 624-631.

(35) Lindfors, T.; Szücs, J.; Sundfors, F.; Gyurcsányi, R. E. *Anal. Chem.* **2010**, *82*, 9425-9432.

(36) Cha, G. S.; Liu, D.; Meyerhoff, M. E.; Cantor, H. C.; Midgley, A. R.; Goldberg, H. D.; Brown, R. B. *Anal. Chem.* **1991**, *63*, 1666-1672.

(37) Piao, M.-H.; Yoon, J.-H.; Jeon, G.; Shim, Y.-B. *Sensors-Basel* **2003**, *3*, 192-201.

(38) Bakker, E. *J. Electroanal. Chem.* **2010**, *639*, 1-7.

(39) Hamer, W. J.; Wu, Y. C. *J. Phys. Chem. Ref. Data* **1972**, *1*, 1047-1100.

(40) Bard, A. J.; Faulkner, L. R. *Electrochemical methods: fundamentals and applications*; Wiley: New York, 2000.

(41) Szigeti, Z.; Vigassy, T.; Bakker, E.; Pretsch, E. *Electroanalysis* **2006**, *18*, 1254-1265.

(42) Bakker, E.; Pretsch, E.; Bühlmann, P. *Anal. Chem.* **2000**, *72*, 1127-1133.

(43) Hu, J.; Stein, A.; Bühlmann, P. *Trends Anal. Chem.* **2016**, *76*, 102-114.

(44) Crespo, G. A.; Macho, S.; Rius, F. X. *Anal. Chem.* **2008**, *80*, 1316-1322.

(45) Österholm, A.; Lindfors, T.; Kauppila, J.; Damlin, P.; Kvarnström, C. *Electrochim. Acta.* **2012**, *83*, 463-470.

(46) Lai, C. Z.; Fierke, M. A.; Stein, A.; Bühlmann, P. *Anal. Chem.* **2007**, *79*, 4621-4626.

(47) Crespo, G. A.; Macho, S.; Bobacka, J.; Rius, F. X. *Anal. Chem.* **2009**, *81*, 676-681.

(48) Ping, J. F.; Wang, Y. X.; Wu, J.; Ying, Y. B. *Electrochem. Commun.* **2011**, *13*, 1529-1532.

(49) Li, F.; Ye, J.; Zhou, M.; Gan, S.; Zhang, Q.; Han, D.; Niu, L. *Analyst* **2012**, *137*, 618-623.

(50) Hernández, R.; Riu, J.; Bobacka, J.; Vallés, C.; Jiménez, P.; Benito, A. M.; Maser, W. K.; Rius, F. X. *J. Phys. Chem. C* **2012**, *116*, 22570-22578.

(51) Yin, T.; Pan, D.; Qin, W. *Anal. Chem.* **2014**, *86*, 11038-11044.

(52) Bieg, C.; Fuchsberger, K.; Stelzle, M. *Anal. Bioanal. Chem.* **2017**, *409*, 45-61.

(53) Cadogan, A.; Gao, Z.; Lewenstam, A.; Ivaska, A.; Diamond, D. *Anal. Chem.* **1992**, *64*, 2496-2501.

(54) Hauser, P. C.; Chiang, D. W. L.; Wright, G. A. *Anal. Chim. Acta* **1995**, *302*, 241-248.

(55) Liu, D.; Meruva, R. K.; Brown, R. B.; Meyerhoff, M. E. *Anal. Chim. Acta* **1996**, *321*, 173-183.

(56) Fouskaki, M.; Chaniotakis, N. *Analyst* **2008**, *133*, 1072-1075.

(57) Fibbioli, M.; Bandyopadhyay, K.; Liu, S. G.; Echegoyen, L.; Enger, O.; Diederich, F.; Bühlmann, P.; Pretsch, E. *Chem. Commun.* **2000**, *5*, 339-340.

(58) Fibbioli, M.; Bandyopadhyay, K.; Liu, S.-G.; Echegoyen, L.; Enger, O.; Diederich, F.; Gingery, D.; Bühlmann, P.; Persson, H.; Suter, U. W.; Pretsch, E. *Chem. Mater.* **2002**, *14*, 1721-1729.

(59) Zou, X. U.; Cheong, J. H.; Taitt, B. J.; Bühlmann, P. *Anal. Chem.* **2013**, *85*, 9350-9355.

(60) Zhou, M.; Gan, S.; Cai, B.; Li, F.; Ma, W.; Han, D.; Niu, L. *Anal. Chem.* **2012**, *84*, 3480-3483.

(61) Hu, J.; Zou, X. U.; Stein, A.; Bühlmann, P. *Anal. Chem.* **2014**, *86*, 7111-7118.

(62) Guimard, N. K.; Gomez, N.; Schmidt, C. E. *Prog. Polym. Sci.* **2007**, *32*, 876-921.

(63) Heinze, J.; Frontana-Uribe, B. A.; Ludwigs, S. *Chem. Rev.* **2010**, *110*, 4724-4771.

(64) Xu, L. B.; Chen, W.; Mulchandani, A.; Yan, Y. S. *Angew. Chem. Int. Ed.* **2005**, *44*, 6009-6012.

(65) Pickup, P. G. In *Mordern aspects of electrochemistry*, White, R. E.; Bockris, J. O. M.; Conway, B. E., Eds.; Kluwer Academic/Plenum Publishers: New York, 1999, pp 549-597.

(66) Inzelt, G. *Conducting polymers: a new era in electrochemistry*, 1st ed.; Springer: New York, 2008.

(67) Akieh, M. N.; Varga, Á.; Latonen, R. M.; Ralph, S. F.; Bobacka, J.; Ivaska, A. *Electrochim. Acta.* **2011**, *56*, 3507-3515.

(68) Chandrasekhar, P. Conducting polymers, fundamentals and applications: a practical approach; Kluwer: Dordrecht, 1999.

(69) Hillman, A. R.; Daisley, S. J.; Bruckenstein, S. *Electrochim. Acta.* **2008**, *53*, 3763-3771.

(70) Zhou, H.; Shi, Z. Q.; Lu, Y. *Synth. Met.* **2010**, *160*, 1925-1930.

(71) Chang, J. H.; Hunter, I. W. *Macromol. Rapid Commun.* **2011**, *32*, 718-723.

(72) Robinson, L.; Isaksson, J.; Robinson, N. D.; Berggren, M. *Surf. Sci.* **2006**, *600*, L148-L152.

(73) Santos, L.; Martin, P.; Ghilane, J.; Lacaze, P. C.; Lacroix, J. C. *ACS Appl. Mater. Interfaces* **2013**, *5*, 10159-10164.

(74) Toth, K.; Lindner, E.; Pungor, E.; Zippel, E.; Kellner, R. *Fresenius' Z. Anal. Chem.* **1988**, *331*, 448-453.

(75) Österholm, A.; Esteban, B. M.; Kvarnström, C.; Ivaska, A. *J. Electroanal. Chem.* **2008**, *613*, 160-170.

(76) Grodzka, E.; Winkler, K.; Esteban, B. M.; Kvarnström, C. *Electrochim. Acta* **2010**, *55*, 970-978.

(77) Osaka, T.; Naoi, K.; Hirabayashi, T. *J. Electrochem. Soc.* **1987**, *134*, 2645-2649.

(78) Schuhmann, W.; Huber, J.; Mirlach, A.; Daub, J. *Adv. Mater.* **1993**, *5*, 124-126.

(79) Lete, C.; Esteban, B. M.; Kvarnström, C.; Razus, A. C.; Ivaska, A. *Electrochim. Acta* **2007**, *52*, 6476-6483.

(80) Wang, F.; Lai, Y. H.; Han, M. Y. *Org. Lett.* **2003**, *5*, 4791-4794.

(81) Neoh, K. G.; Kang, E. T.; Tan, T. C. *Polym. Bull.* **1988**, *19*, 325-331.

(82) Porsch, M.; Sigl-Seifert, G.; Daub, J. *Adv. Mater.* **1997**, *9*, 635-639.

(83) Bargon, J.; Mohmand, S.; Waltman, R. J. *Mol. Cryst. Liq. Cryst.* **1983**, *93*, 279-291.

(84) Nie, G.; Cai, T.; Zhang, S.; Hou, J.; Xu, J.; Han, X. *Mater. Lett.* **2007**, *61*, 3079-3082.

(85) Latonen, R. M.; Österholm, A.; Kvarnström, C.; Ivaska, A. *J. Phys. Chem. C* **2012**, *116*, 23793-23802.

(86) Diaz, A. F.; Kanazawa, K. K.; Gardini, G. P. *J. Chem. Soc. Chem. Commun.* **1979**, 635-636.

(87) Kang, H. C.; Geckeler, K. E. *Polymer* **2000**, *41*, 6931-6934.

(88) Baughman, R. H. *Science* **2005**, *308*, 63-65.

(89) Bobacka, J. *Electroanalysis* **2006**, *18*, 7-18.

(90) Bobacka, J.; Ivaska, A.; Lewenstam, A. *Electroanalysis* **2003**, *15*, 366-374.

(91) Ramanavičius, A.; Ramanavičienė, A.; Malinauskas, A. *Electrochim. Acta.* **2006**, *51*, 6025-6037.

(92) Rubinova, N.; Chumbimuni-Torres, K.; Bakker, E. *Sens. Actuators, B* **2007**, *121*, 135-141.

(93) Gyurcsányi, R. E.; Rangisetty, N.; Clifton, S.; Pendley, B. D.; Lindner, E. *Talanta* **2004**, *63*, 89-99.

(94) Michalska, A.; Hulanicki, A.; Lewenstam, A. *Microchem. J.* **1997**, *57*, 59-64.

(95) Sutter, J.; Lindner, E.; Gyurcsányi, R. E.; Pretsch, E. *Anal. Bioanal. Chem.* **2004**, *380*, 7-14.

(96) Maksymiuk, K. *Electroanalysis* **2006**, *18*, 1537-1551.

(97) Bobacka, J.; Alaviuhkola, T.; Hietapelto, V.; Koskinen, H.; Lewenstam, A.; Lämsä, M.; Pursiainen, J.; Ivaska, A. *Talanta* **2002**, *58*, 341-349.

(98) Sutter, J.; Radu, A.; Peper, S.; Bakker, E.; Pretsch, E. *Anal. Chim. Acta* **2004**, *523*, 53-59.

(99) Vazquez, M.; Bobacka, J.; Ivaska, A.; Lewenstam, A. *Sens. Actuators, B* **2002**, *82*, 7-13.

(100) Mousavi, Z.; Bobacka, J.; Ivaska, A. *Electroanalysis* **2005**, *17*, 1609-1615.

(101) Lindfors, T.; Ivaska, A. *Anal. Chem.* **2004**, *76*, 4387-4394.

(102) Lindfors, T.; Latonen, R. M. *Carbon* **2014**, *69*, 122-131.

(103) Lindfors, T. *J. Solid State Electrochem.* **2009**, *13*, 77-89.

(104) Craggs, A.; Moody, G. J.; Thomas, J. D. R. *J. Chem. Educ.* **1974**, *51*, 541-544.

(105) Horvai, G.; Graf, E.; Toth, K.; Pungor, E.; Buck, R. P. *Anal. Chem.* **1986**, *58*, 2735-2740.

(106) Püntener, M.; Fibbioli, M.; Bakker, E.; Pretsch, E. *Electroanalysis* **2002**, *14*, 1329-1338.

(107) Li, Z.; Li, X.; Petrovic, S.; Harrison, D. J. *Anal. Chem.* **1996**, *68*, 1717-1725.

(108) Sundfors, F.; Lindfors, T.; Höfler, L.; Bereczki, R.; Gyurcsányi, R. E. *Anal. Chem.* **2009**, *81*, 5925-5934.

(109) Lindfors, T.; Sundfors, F.; Höfler, L.; Gyurcsányi, R. E. *Electroanalysis* **2009**, *21*, 1914-1922.

(110) Li, Z.; Li, X.; Rothmaier, M.; Harrison, D. J. *Anal. Chem.* **1996**, *68*, 1726-1734.

(111) Lindfors, T.; Sundfors, F.; Höfler, L.; Gyurcsányi, R. E. *Electroanalysis* **2011**, *23*, 2156-2163.

(112) Lindfors, T.; Höfler, L.; Jágerszki, G.; Gyurcsányi, R. E. *Anal. Chem.* **2011**, *83*, 4902-4908.

(113) Li, Y.; Qian, R. *Synth. Met.* **1993**, *53*, 149-154.

(114) Maksymiuk, K.; Bobacka, J.; Ivaska, A.; Lewenstam, A. *Anal. Lett.* **2000**, *33*, 1339-1360.

(115) Lindfors, T.; Ivaska, A. *J. Electroanal. Chem.* **2002**, *531*, 43-52.

(116) Grummt, U.-W.; Pron, A.; Zagorska, M.; Lefrant, S. *Anal. Chim. Acta* **1997**, *357*, 253-259.

(117) Freiser, H. *Ion-selective electrodes in analytical chemistry*; Plenum Press, New York, 1978.

(118) Zou, X. U.; Zhen, X. V.; Cheong, J. H.; Bühlmann, P. *Anal. Chem.* **2014**, *86*, 8687-8692.

(119) Vanamo, U.; Bobacka, J. *Electrochim. Acta.* **2014**, *122*, 316-321.

(120) Vanamo, U.; Bobacka, J. *Anal. Chem.* **2014**, *86*, 10540-10545.

(121) Guzinski, M.; Jarvis, J. M.; Pendley, B. D.; Lindner, E. *Anal. Chem.* **2015**, *87*, 6654-6659.

(122) Fischer, K. *Angew. Chem.* **1935**, *48*, 394-396.

(123) Larsson, W.; Jalbert, J.; Gilbert, R.; Cedergren, A. *Anal. Chem.* **2003**, *75*, 1227-1232.

(124) Kvarnström, C.; Ivaska, A.; Neugebauer, H. *Advanced functional molecules and polymers*, Nalwa, H. ed.; Gordon & Breach Science Publishers: Australia, 2001; Vol. 2, Ch.6.

(125) Vo-Dinh, T.; Gauglitz, G. *Handbook of Spectroscopy*; Wiley-VCH, Weinheim, 2003; Vol. 1.

(126) Socrates, G. Infrared and Raman Characteristic Group Frequencies: Tables and Charts, 3 ed.; John Wiley & Sons Ltd: Chichester, 2001.

(127) Neugebauer, H.; Ping, Z. In Progress in Fourier Transform Spectroscopy: Proceedings of the 10th International Conference, August 27 – September 1, 1995, Budapest, Hungary, Mink, J.; Keresztury, G.; Kellner, R., Eds.; Springer Vienna: Vienna, 1997, pp 125-131.

(128) Griffiths, P.; De Haseth, J. *Fourier transform infrared spectrometry*, 2 ed.; Wiley-Interscience: Hoboken, N. J., 2007, p 321-347.

(129) Willard, H. H.; Merritt, L. L., Jr.; Dean, J. A.; Settle, F. A., Jr. *Instrumental methods of analysis*; Wadsworth: Belmont, CA, 1988, p 713-715.

(130) Brett, C. M. A.; Brett, A. M. O. *Electrochemistry Principles, Methods, and Applications*; Oxford University Press, 1993.

(131) Young, T. *Philos. Trans. R. Soc. London* **1805**, *95*, 65-87.

(132) Wenzel, R. N. *Ind. Eng. Chem.* **1936**, *28*, 988-994.

(133) He, N.; Lindfors, T. *Anal. Chem.* **2013**, *85*, 1006-1012.

(134) He, N.; Höfler, L.; Latonen, R. M.; Lindfors, T. *Sens. Actuators, B* **2015**, *207*, 918-925.

(135) He, N.; Papp, S.; Lindfors, T.; Höfler, L.; Latonen, R. M.; Gyurcsányi, R. E. *Anal. Chem.* **2017**, *89*, 2598-2605.

(136) Bakker, E. *Anal. Chem.* **2015**.

(137) Liu, M. J.; Tzou, K.; Gregory, R. V. *Synth. Met.* **1994**, *63*, 67-71.

(138) Bobacka, J. *Anal. Chem.* **1999**, *71*, 4932-4937.

(139) He, N.; Gyurcsányi, R. E.; Lindfors, T. *Analyst* **2016**, *141*, 2990-2997.

(140) Paczosa-Bator, B. *Talanta* **2012**, *93*, 424-427.

(141) Zhong, C.; Doblhofer, K. *Electrochim. Acta.* **1990**, *35*, 1971-1976.

(142) Sundfors, F.; Höfler, L.; Gyurcsányi , R. E.; Lindfors , T. *Electroanalysis* **2011**, *23*, 1769-1772.

(143) Sutter, J.; Pretsch, E. *Electroanalysis* **2006**, *18*, 19-25.

(144) Vazquez, M.; Danielsson, P.; Bobacka, J.; Lewenstam, A.; Ivaska, A. *Sens. Actuators, B* **2004**, *97*, 182-189.

Cover picture drawn by Qi Baishi

ISBN: 978-952-12-3594-8
Painosalama Oy - Åbo, Finland 2017